② LEVEL Ⅲ *AD-E ͆₀₀495*

ADA086089

HIGH BANDWIDTH, FINE RESOLUTION DEFORMABLE MIRROR DESIGN

Ralph E. Aldrich
Jeffrey H. Everson
Nedo P. Albertinetti

Itek, Optical Systems Division
Lexington, MA 02173

March 1980

Final Report

DTIC
ELECTE
JUL 1 1980

B

AIR FORCE WEAPONS LABORATORY
Air Force Systems Command
Kirtland Air Force Base, NM 87117

DDC FILE COPY

80 4 28 067

This final report was prepared by Itek Corporation, Optical Systems Division, Lexington, Massachusetts, under Contract F29601-78-C-0060, Job Order ILIR 7308 with the Air Force Weapons Laboratory, Kirtland Air Force Base, New Mexico. Dr. John R. Kenemuth was the Laboratory Project Officer-in-Charge.

When US Government drawings, specifications, or other data are used for any purpose other than a definitely related Government procurement operation, the Government thereby incurs no responsibility nor any obligation whatsoever, and the fact that the Government may have formulated, furnished, or in any way supplied the said drawings, specifications, or other data, is not to be regarded by implication or otherwise, as in any manner licensing the holder or any other person or corporation, or conveying any rights or permission to manufacture, use, or sell any patented invention that may in any way be related thereto.

This report has been authored by a contractor of the United States Government. The United States Government retains a nonexclusive, royalty-free license to publish or reproduce the material contained herein, or allow others to do so, for United States Government purposes.

This report has been reviewed by the Public Affairs and is releasable to the National Technical Information Service (NTIS). At NTIS, it will be available to the general public, including foreign nations.

This technical report has been reviewed and is approved for publication.

DR. JOHN R. KENEMUTH
Project Officer

FOR THE DIRECTOR

MILTON L. CONE   ARMAND D. MAIO
Major, USAF   Colonel, USAF
Acting Chief, Adv Beam Control Br   Chief, Advanced Laser Technology
                                            Division

DO NOT RETURN THIS COPY.   RETAIN OR DESTROY.

REPORT DOCUMENTATION PAGE	READ INSTRUCTIONS BEFORE COMPLETING FORM

1. REPORT NUMBER	2. GOVT ACCESSION NO.	3. RECIPIENT'S CATALOG NUMBER
AFWL-TR-79-5	✓ AD-A086 089	

4. TITLE (and Subtitle)	5. TYPE OF REPORT & PERIOD COVERED
HIGH BANDWIDTH, FINE RESOLUTION DEFORMABLE MIRROR DESIGN	Final Report
	6. PERFORMING ORG. REPORT NUMBER 8432

7. AUTHOR(s)	8. CONTRACT OR GRANT NUMBER(s)
Ralph E. Aldrich Jeffrey H. Everson Nedo P. Albertinetti	F29601-78-C-0060

9. PERFORMING ORGANIZATION NAME AND ADDRESS	10. PROGRAM ELEMENT, PROJECT, TASK AREA & WORK UNIT NUMBERS
Itek, Optical Systems Division Lexington, MA. 02173	61101F/ILIR7808

11. CONTROLLING OFFICE NAME AND ADDRESS	12. REPORT DATE
Air Force Weapons Laboratory (ARAA) Kirtland Air Force Base, NM 87117	March 1980
	13. NUMBER OF PAGES 70

14. MONITORING AGENCY NAME & ADDRESS(if different from Controlling Office)	15. SECURITY CLASS. (of this report)
	UNCLASSIFIED
	15a. DECLASSIFICATION/DOWNGRADING SCHEDULE

16. DISTRIBUTION STATEMENT (of this Report)

Approved for public release; distribution unlimited.

17. DISTRIBUTION STATEMENT (of the abstract entered in Block 20, if different from Report)

18. SUPPLEMENTARY NOTES

19. KEY WORDS (Continue on reverse side if necessary and identify by block number)

Deformable mirror	Multilayer actuator
Corrector mirror	Honeycomb actuator
Coherent stack actuator	Tubular actuator
Bimorph actuator	

20. ABSTRACT (Continue on reverse side if necessary and identify by block number)

This report describes the design, fabrication and testing of five candidate actuator types to achieve a deformable mirror capable of 6 microns dilatation at 1.5 kV. The actuator types are the coherent stack, bimorph, tube, multilayer and the honeycomb.

DD $_{1 \text{ JAN } 73}^{\text{FORM}}$ 1473

Table of Contents

List of Figures

List of Tables

List of Photographs

I INTRODUCTION

This document is the final report which details the technical progress achieved under the program entitled, "High Bandwidth, Fine Resolution Deformable Mirror Design" (contract F29601-78-C-0060). Based upon the goals listed in Table 1, this program entailed the design, fabrication and characterization of five deformable surface devices. These devices employ actuators constructed from piezoelectric ceramics either in the form of multilayers, honeycombs, tubes, bimorphs or coherent stacks. The acceptance or rejection of potential actuator types was accomplished on the basis of sensitivity, material availability, fabrication techniques, response and stability. Meeting and in some cases significantly exceeding the program goals, the five device types presented in this report represent a broad data base upon which a final device candidate may be chosen.

Following a brief summary of the reasons for device acceptance or rejection in section two, this report provides a discussion of each candidate device type in a separate section. The individual sections generally present construction details, electrical properties, dilatational measurements, characterization of mechanical resonance and life testing. Appendix A outlines the methods of resonance measurment. Summarized in Appendix B are several technical problems which arose during the course of the program.

TABLE 1. PROGRAM GOALS FOR DEFORMABLE MIRROR

Active Diameter	20 cm
Surface Flatness	$\lambda/20$ rms at 4 μm
Maximum Surface Dilatation	±6 μm
Maximum Interactuator Dilatation	±6 μm
Operating Bandwidth	DC - 1000 Hz
Maximum Voltage	1500 V
Actuator Spacing	~2.5 cm
Actuator Geometry and Type	To be determined
Operating Temperature Range	0° - 50° C

II CONCEPT SELECTION

The first task of this program was to select a group
of concepts which could potentially satisfy the goals of
the program. No restriction was placed on present level
of development, but concepts selected would have to prove
a theoretical potential capability adequate to meet these
goals. Thus, a master listing of device structures was
prepared limited only by the requirement that these devices
use piezoelectric materials as the active element. A total
of eleven structures were evaluated in terms of known or
potential sensitivity, voltage limitations, stability, dif-
ficulty of fabrication, and availability of materials. Each
of these structures is discussed briefly below, together with
whatever reasons for rejection were considered most significant.
Schematic diagrams for all devices are shown in Figure 1.

1   Monolithic Piezoelectric Mirror (MPM)

The MPM is a standard Itek device for correction of
visible light. The device is monolithic, extremely stable,
has demonstrated excellent wavefront correction capability
and can be operated at frequencies up to 100 kHz. It utilizes
the longitudinal deformation of a PZT substrate to bend a mirror
locally. Substrates 15 cm in diameter are readily available
and 20 cm diameter can be produced relatively easily. However,
the major problem is device sensitivity. This device has a
sensitivity between 1.5 and 4.5 $\overset{o}{A}$/V, depending on the details
of the electrode geometry, faceplate, etc. Exhaustive tests
have indicated that a practical limit is reached between 4 and
5 $\overset{o}{A}$/V. Since program goals require 6 μm at 1500 V (40 $\overset{o}{A}$/V)
this device is not suitable for further study.

2   "Moat" Mirror

The moat device is essentially a MPM with a floating face-
plate. Sensitivity of the device is increased to approximately

3

Electrode

PZT block

(a) Monolithic piezoelectric
mirror (MPM)
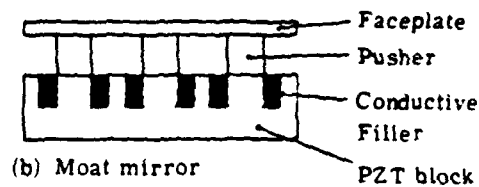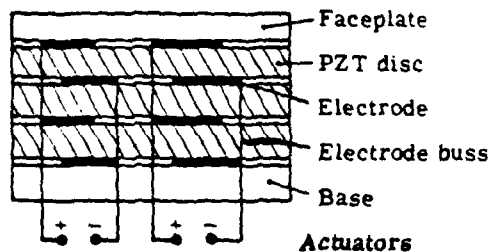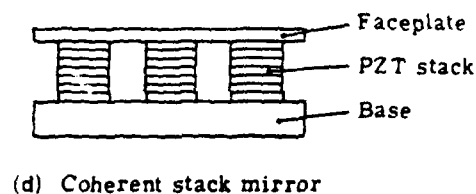
Faceplate
Pusher
Conductive
Filler
PZT block

(b) Moat mirror

Faceplate
PZT disc
Electrode
Electrode buss
Base
Actuators

(c) Brick wall mirror

Faceplate
PZT stack
Base

(d) Coherent stack mirror

Faceplate
PZT disc
Electrode
PZT disc

(e) Continuous plate bimorph mirror

Faceplate
Pusher
PZT bimorph
Clamp
Base

(f) Discrete bimorph mirror

Faceplate
Pusher
Tube
Base

(g) Single tube mirror

Faceplate
Pusher
Tubes
Bonds
Base
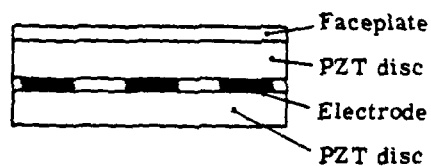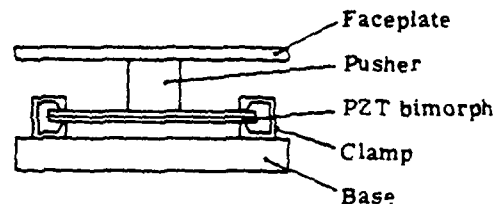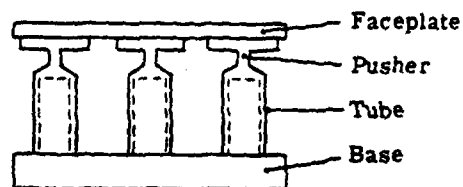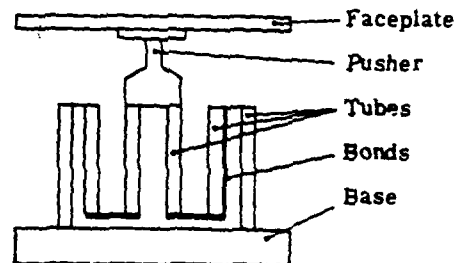
(h) Nested tubular array mirror
(cross section, one actuator)

PZT

Electrodes
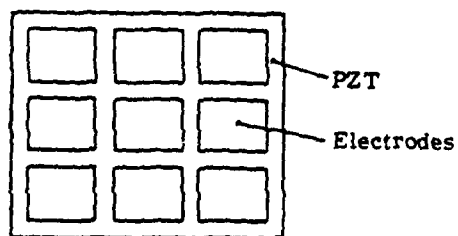
(i) Honeycomb mirror (top view)

Figure 1 – Deformable mirror design

4

7 $\overset{\circ}{A}$/V by the use of a conductive filler in the moat. However, there appears to be no method of increasing the sensitivity to the necessary minimum; hence, this device was not pursued.

3   "Brick Wall" Piezoelectric Mirror

This device is constructed by bonding several piezoelectric disks, which have been previously electroded in the manner shown in Figure 1C. Holes are then drilled in the bonded disks so that the electrode bus wires can contact alternating electrodes. The poling direction of a disk is opposite to that of the adjacent disks. Thus, the actuator is connected electrically in parallel to achieve a series dilatation. This device may be thought of as a coherent stack which is not cut into discrete actuator stacks.

Previous data indicated a sensitivity of 13 $\overset{\circ}{A}$/V for a structure composed of 8 layers of PZT each 2 mm thick. The device has all the stability characteristics of the MPM. The critical point is that doubling the number of layers had no effect on sensitivity. Since each layer must deform all layers above it, the effective stiffness of the device increases for each layer until finally the layers are completely pinned. Apparently this limit is reached at 8 layers (1.6 cm thickness). Sensitivity can in theory be increased by using thinner layers but the effect will be inadequate for the following reason. The maximum safe field to be applied to PZT based on the poling conditions is 10^4 V/cm. A free wafer of low hysteresis PZT has a sensitivity of approximately 2.5 $\overset{\circ}{A}$/V. Thus, the minimum actuator length required to obtain 6 μm of throw is 2.4 cm. Thus, even if the sensitivity could be increased to 40 $\overset{\circ}{A}$/V, the maximum deflection before breakdown would be no greater than 4 μm.

4   Coherent Stack Mirror

This device is assembled by laminating together layers of PZT to obtain an increase in sensitivity. The requirement

5

is like that shown in section 3. A minimum actuator length
of 2.4 cm is required. Available data on a 16 layer stack
indicated a sensitivity of 35 $\overset{o}{A}$/V scaleable simply by in-
creasing the number of layers. In addition the device is
relatively easy to fabricate. Although there remained serious
questions of stability, uniformity, and resonances, it was
believed that there were no fundamental limitations in this
actuator structure. Thus, this device was selected for
further study.

5 Continuous Plate Bimorph Mirror

This device relies on the transverse component of the
piezoelectric effect for its operation. The applied field
causes a layer of PZT to increase in diameter and the other
to decrease in diameter. This has the effect of bending the
entire plate structure. Sensitivities of 15 $\overset{o}{A}$/V have been
measured. However, it appears unlikely that the sensitivity
can be increased by a factor of three. Further the entire
device bends when any actuator is driven, thus producing a
very complex problem in wavefront correction. Such a device
appears more useful as a focus corrector, an application where
the radial symmetry of the deformation can be an advantage.

6 Discrete Bimorph Mirror

The discrete bimorph relies on bimorph bending as does
the continuous plate bimorph, but in this case the actuators
are discrete and act on the mirror by means of a pusher which
joins the bimorph element to the mirror. Very high sensitivi-
ties (80 $\overset{o}{A}$/V) have been measured. However, this actuator is
a low force device, very sensitive to faceplate stiffness.
This device was chosen for further study even though virtually
nothing was known about its mechanical properties or stability.
However, it does satisfy the other requirements, and appears
to have some potential.

6

7   Single Tube Mirror

This device uses actuators composed of PZT tubes with
the voltage applied through the wall thickness. This actuator
is a transverse field device as are the bimorphs. Since the
tube diameter changes when the actuator is driven, a diameter
independent flexure must be used to join the actuator and the
faceplate. Data indicated an anticipated sensitivity of
8 $\overset{o}{A}$/V/cm of tube length for a reasonable geometry, hence a
5 cm long tube should have adequate sensitivity. In addition,
the tubular structure is extremely stable, making this device
a potential candidate.

8   Nested Tubular Array Mirror

The structure is similar to the single tube mirror except
that several tubes are nested one within the other and bonded
alternately top and bottom to achieve the effect of a long
tube but with a very short (1-2 cm) actuator. This device
is felt to have potentially desirable mechanical properties
but was not studied on the program because time was limited
and our instructions were to examine only tubular actuators.

9   Honeycomb Structure Mirror

The honeycomb format is a method for creating a long throw
device while maintaining a monolithic structure and the mechanical
and thermal advantages which result from that structure. The
device was totally new and fabrication was seen as a significant
problem. Only limited data could be taken due to the nonavail-
ability of appropriate test samples. Fabrication of this structure
remains the most significant problem.

10   Multilayer Actuator Mirror

This is an analagous structure to the coherent stack
except that the layers are very thin (typically 0.25 mm).
The total number of layers is large, generally 100 or more

being used to make up the stack. Electrostrictive materials such as lead magnesium niobate having no hysteresis can be used as well as standard ferroelectric PZT compositions. Potential operating voltage is very low, typically 200 V. The major limitation in this type of actuator is that the fabrication technology is still in its infancy.

11 Tree Ring Mirror

An actuator similar to the multilayer actuator but formed in concentric rings and thus using the transverse effect to produce a deformation. This device should be a low votage analog of the tubular array. No suitable supplier of this structure, even in single unit quantities, has been found.

12 Summary

As a result of this work five devices were selected for further study. They are the coherent stack, discrete bimorph, single tube, honeycomb, and multilayer. Four designs, the MPM, moat mirror, brick wall and continuous plate bimorph were rejected for inadequate sensitivity. The remaining three were not pursued due to anticipated fabrication problems or the unavailability of materials.

III MULTILAYER ACTUATOR

Two multilayer actuators, obtained from our consultant, Professor Leslie E. Cross at Penn State, consist of 10 elements each. Each element has 10 internal layers of piezoelectric ceramic (PZT-8 composition). Each layer is made by a tape casting procedure which has been perfected at Penn State.

A sensitivity plot, provided by Professor Cross, is given in Figure 2. The vertical axis is given in terms of strain ($\Delta L/L$), while the horizontal scale measures electric field (volts per meter). Our measurements show that 200 volts applied to the multilayer yields approximately 3 µm displacement with no bonded face plate. The capacitance is about 300 nF for the entire stack, which exhibited a loss tangent of 0.002. (See Appendix C for a discussion of capacitance measurement.)

1   Influence Function

Shown in Figure 3 is the influence function (i.e., deformation measured by surface profilometer at discrete points extending radially from the energized actuator). The device (#165) consists of nine elements, one multilayer stack surrounded by eight aluminum posts. Two hundred volts were applied to this device which was equipped with a glass face plate having a thickness of 0.17 cm.

Since these multilayer stacks arrived rather late during the program it was not possible to undertake more extensive characterization with them. Although Professor Cross has made numerous material advancements, he is not really equipped to deal with production problems. The fact that multilayer technology provides a great deal of dilatation for a relatively modest voltage (150 $\overset{\circ}{A}$/V) suggests an engineering/production program would be an attractive, low risk venture, which would require only a transfer of well developed technology between Penn State and Itek.

9

Dilatation ($\Delta S = \Delta L/L$ X10^{-5})

16

14

12

10

8

6

4

2

0

                • = trial 1

                X = trial 2

$d_{33} = \dfrac{\Delta S}{\Delta E} = 223 \times 10^{-12} \text{m/V}$

1   2   3   4   5   6   7   8

Electric field, E (kV/cm)
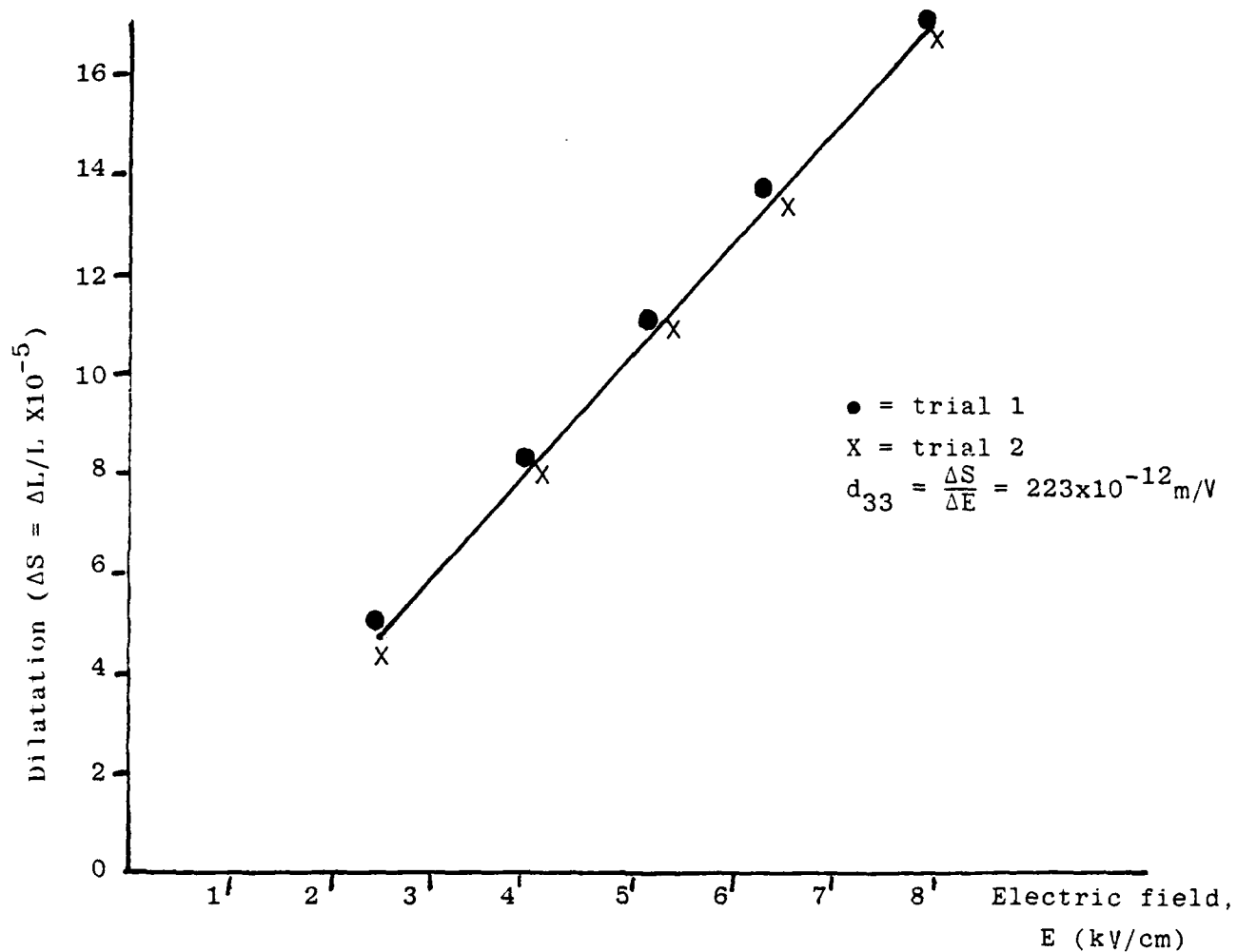
Figure 2 – Multilayer actuator: Dilatation versus applied
                    electric field

10

Actuator Construction

An actuator consists of 10 "sub" stacks bonded in a criss-cross manner. Each "sub" has the following dimensions:

Sub stack
- Length = 2.1 cm
- Width = 0.72 cm
- Thickness = 0.22 cm

Stack
- Length of center stack = 10x0.22 cm

ACTUATOR ARRAY

Position of cylindrical pusher between multilayer actuator and glass faceplate (pusher diameter ≈ 0.64 cm)

2.5 cm

←—2.5 cm—→ Aluminum post (diameter = 0.64 cm)

faceplate thickness is 0.17 cm

200 volts
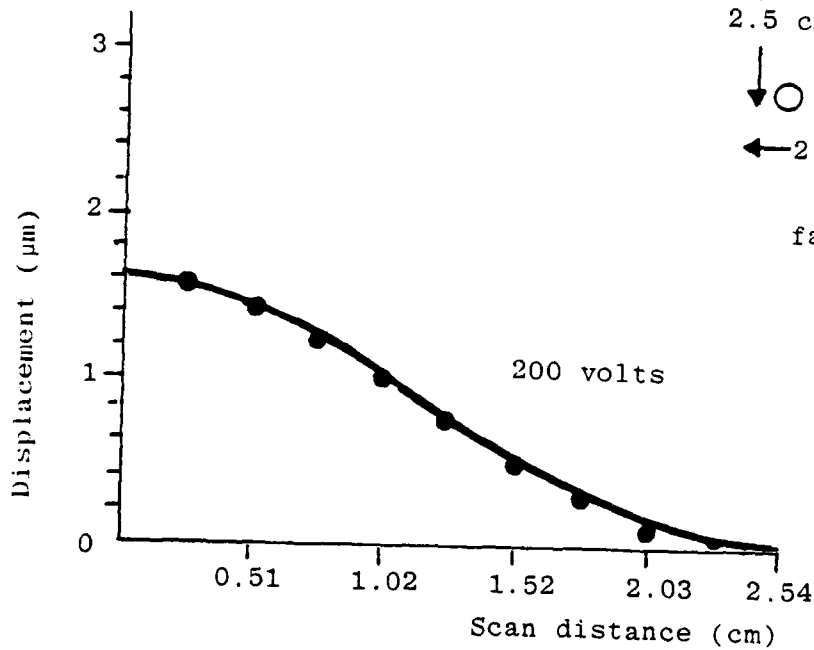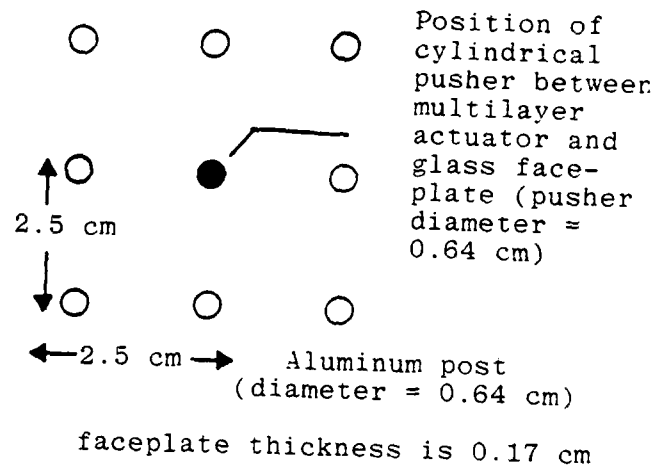
Figure 3 - Multilayer actuator: Influence function

11

IV   HONEYCOMB ACTUATORS

A unique structure referred to as a honeycomb was investigated during this program. Having an overall tubular shape, the device has an interior in the form of a rectangular or triangular honeycomb. Operation of the device relies upon a voltage drop across a honeycomb wall to achieve a transverse surface displacement.

Two samples of a barium titanate honeycomb structure were obtained from Professor Leslie Cross of Penn State. Barium titanate was used because it was available while a PZT honeycomb was not obtainable. Fabrication was prohibited by time and cost considerations. The barium titanate is a modified composition, which has additives to achieve an electrostrictive formulation and was extruded by Corning Glass. Electrodes were applied at Itek by drawing a wire dipped in silver paste through the honeycombs. Cell sizes and wall thicknesses were determined using a measuring microscope. Glass was bonded to each honeycomb to provide a reflective surface.

Table 2 lists the construction details, while Table 3 provides a summary of material properties. The quantities, capacitance (farads), loss tangent and breakdown voltage were measured at Itek after the structures had been electroded. Professor Cross provided us with the electrostrictive constant (Q) and the permittivity value.

1   Electrical Measurements

The measured capacitance displayed a large standard deviation, while on the other hand, the measured sensitivity indicated considerably less deviation about the average value. (See Appendix C for details on capacitance measurement.) The behavior of the standard deviation for the capacitance and sensitivity may be due to the fact that capacitance is obtained

TABLE 2.   HONEYCOMB ACTUATOR: CONSTRUCTION DATA

Cell Size	0.158 cm
Wall Thickness:	0.032 cm
Length:	4.13 cm (Device #157) 6.03 cm (Device #159)
Mirror Thickness:	0.25 mm (Device #157) 1.00 mm (Device #159)

TABLE 3.   HONEYCOMB ACTUATOR: MATERIAL PROPERTIES

Material: Barium Titanate (Electrostrictive)

Electrostrictive Constant: $Q_{12} = \dfrac{S_{22}}{P_1^2} = 0.45 \times 10^{-2} \dfrac{M^4}{C^2}$

S = strain; P = polarization

Permittivity: 3700 @ Room Temperature

Capacitance: Average = 517 pF
                          Standard Deviation = 403 pF

Loss Tangent: 0.05

Breakdown Voltage: 600 V (noncatastrophic)

using an ac measurement while the sensitivity is measured by a dc technique. Under ac conditions the variation in the air gap (between the honeycomb wall surface and the electroding material) may have had a more pronounced effect for the capacitance measurement than the sensitivity measurement.

2   Dilatational Response

Presented in Figure 4 is a log-log plot of dilatation versus applied voltage. The slope of the curve is two up to 200 volts and is one from 200 to 500 volts. Breakdown, which occurred at 600 volts, corresponds to a field of $2.0X10^4$ V/cm. Cell size of this device was 0.158 cm center-to-center with 0.03 cm wall thickness. A slope of two arises from the electrostrictive effect, whereby the dilatation is proportional to the square of the electric field. The slope change to a value of one is due to a saturation of the dielectric constant.

The influence functions were measured by means of a surface profilometer, which determined the amount of surface deformation at regular intervals extending radially from the center of an energized actuator. Figure 5 shows the influence function measured in the direction of the adjacent actuator (scan from actuator #5 to #6) and the influence function obtaind by scanning to the next nearest neighbor from actuator #5 (i.e., #3). The glass thickness was 0.25 mm. Figure 6 displays the influence function for a honeycomb which has a thicker glass faceplate (1.0 mm). For both Figures 5 and 6 it is evident that the overlap at the adjacent (unenergized) actuator is considerable. The result is due to the fact that only a few of the honeycombs were electroded. Normally all honeycombs would be electroded and all unused actuators would be at ground potential. However, the matter was not pursued further.

Although the elongation provided by these particular honeycomb samples does not meet the program goals, it is apparent that more sensitive material (i.e., PZT), structured in a
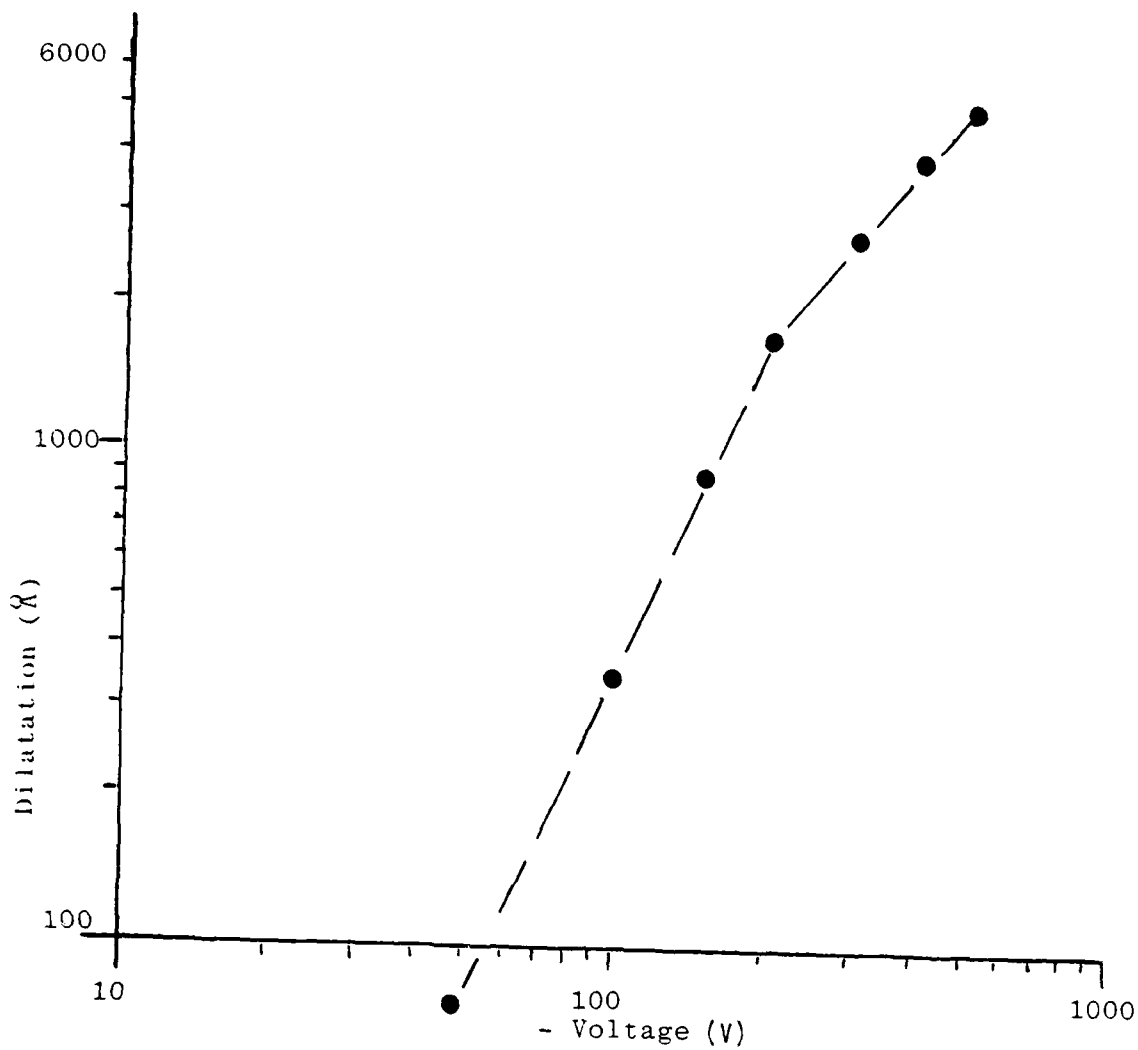
Figure 4 - Honeycomb device (#157): Dilatation versus applied voltage. The center actuator is at negative potential while surrounding actuators (8) are at ground

15
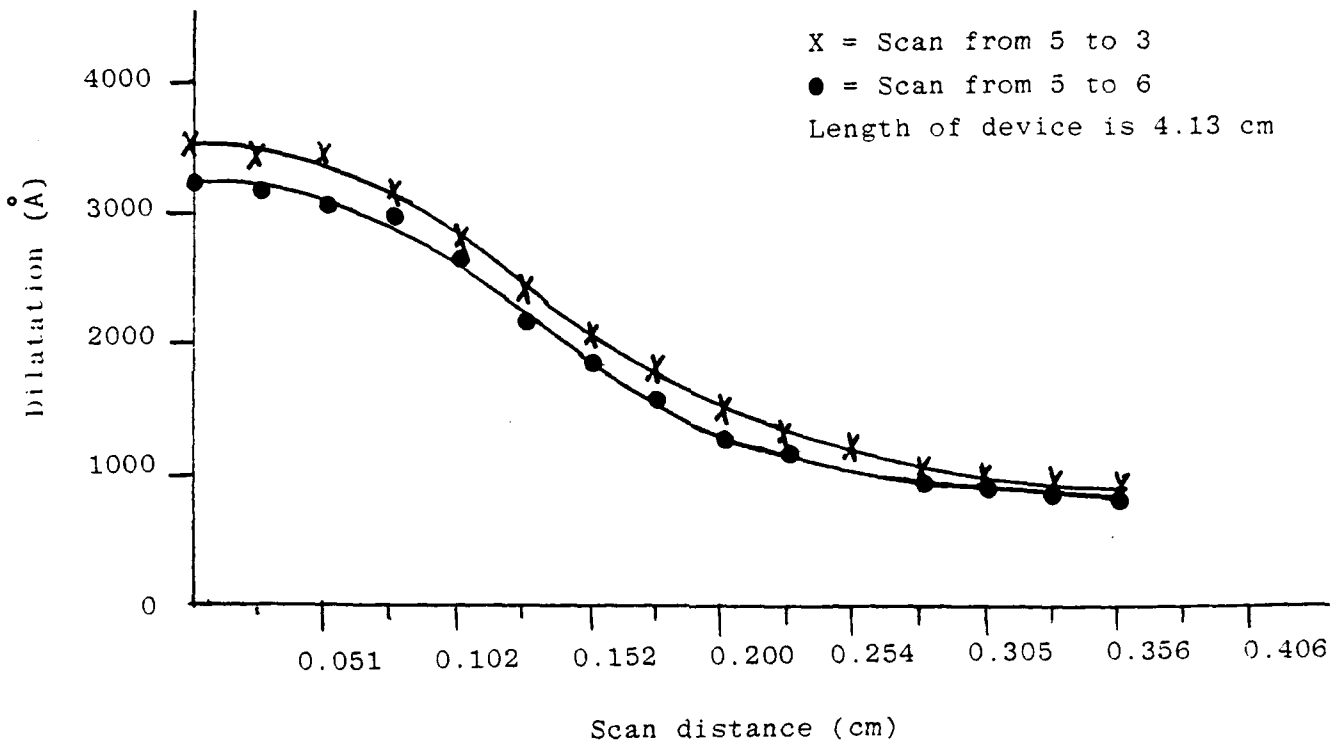
Figure 5 - Honeycomb (device #157): Influence function (glass
thickness is 0.25 mm)
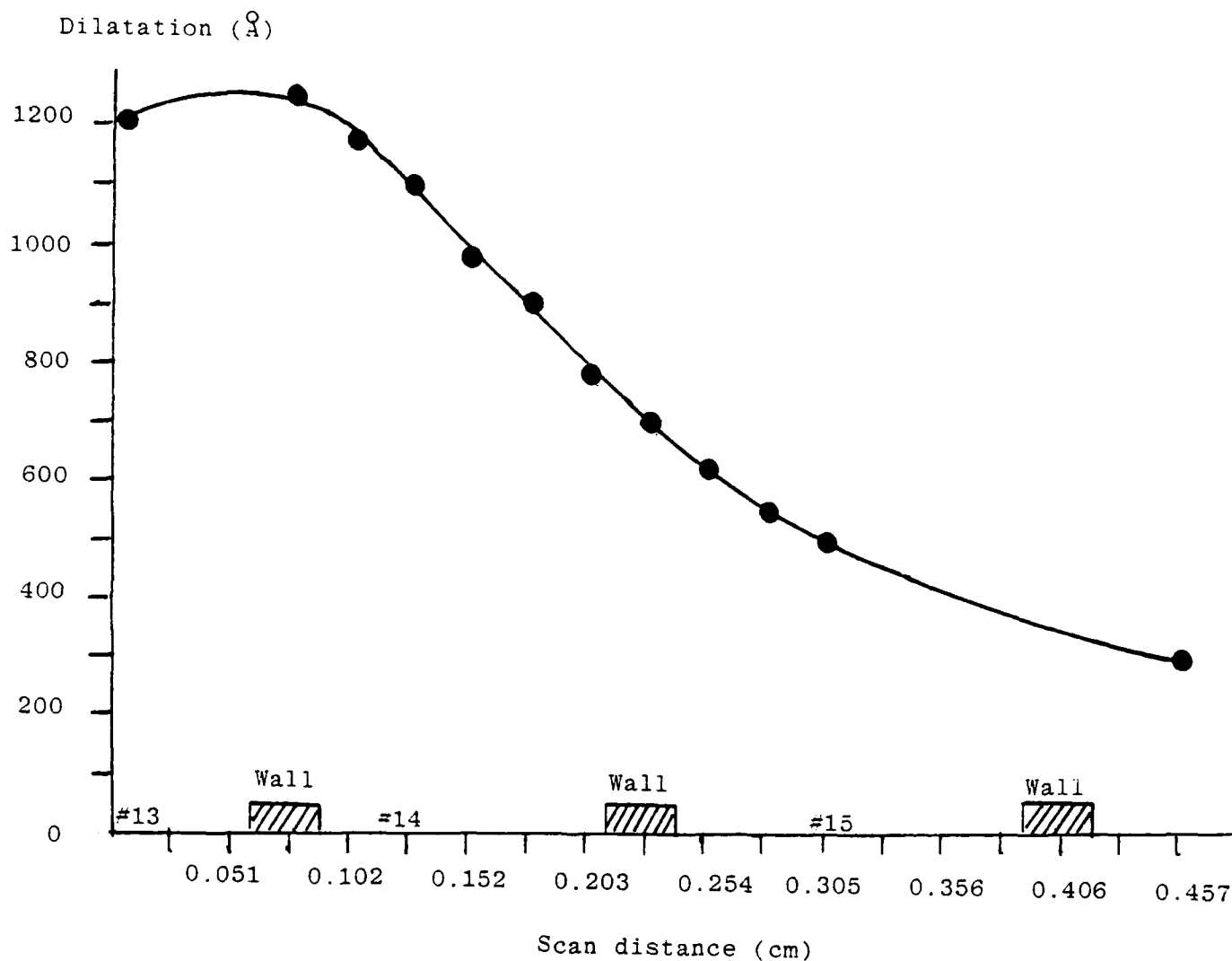
Figure 6 – Honeycomb device (#159): Influence function (glass thickness is 1.00 mm). Central actuator (#11) is at +500 volts, all others are grounded. Actuator array consists of 21 elements. Length of device is 6.03 cm. The array is a 5x5 square, without the corner elements.

honeycomb, would yield an attractive candidate for maximum throw at low voltage. For example, consider the material, PZT-4, which has a transverse piezoelectric coefficient (d_{31}) equal to $96\text{X}10^{-12}$ m/V. Assume a honeycomb, made from PZT-4, has a wall thickness of 1 mm and a length of 75 mm. Using a maximum allowable voltage of 1 kV, the dilatation would be 7 μm or equivalently, the sensitivity would equal 72 Å/V for a honeycomb with no mechanical loading due to a face plate. The sensitivity of the barium titanate device (unloaded) is approximately 10 Å/V. As a point of reference, the state-of-the-art sensitivity for Itek's monolithic piezoelectric mirror (MPM) is approximately 4 Å/V (includes glass face plate of about 0.13 cm thickness). The estimated sensitivity of an MPM with no face plate is 5 Å/V.

V   BIMORPH ACTUATOR

A deformable mirror (#156) using bimorph actuators has
been developed in an effort to provide greater deformation
at reasonable voltages, maintain thermal and mechanical sta-
bility, and operate with a bandwidth of 1 kilohertz. The
bimorph actuator consists essentially of two bonded rectangular
plates which are constructed from a piezoelectric ceramic.
This type of material undergoes a mechanical deformation in
the presence of an electric field. In the case of the bimorph,
the applied voltage causes one plate to expand (i.e., trans-
versely), while the other contracts, thereby causing a bending
effect. The polarity of the applied voltage may be reversed to
cause bending in the opposite sense. For a given voltage, the
amount of displacement is proportional to the length of the
bimorph element. The lever action of the bimorph generates
displacements considerably greater than a single plate but
provides less force.

The bimorph-actuator mirror was characterized in terms
of actuator capacitance (and loss tangent), surface deformation
profile (influence function), sensitivity, linearity of response,
mechanical resonances and long term stability during continuous
operation. The following sections comment upon each of these
properties.

1   Structural Configuration

A bimorph actuator, which consists of the base plate,
bimorph element (PZT), clamp, pusher and face plate is shown
in Figure 7. The bimorph bender is held by a spring loaded
clamp with a curved edge to allow flexural motion. Other holder
designs, using flat clamping surfaces, proved unsuccessful. It
was found that 30 in-lb was sufficient torque for the clamping
bolts to allow bending but also provide mechanical stability.
Each mounting pad was machined from the stainless steel base
plate. Additional construction data is given in Table 4.

19
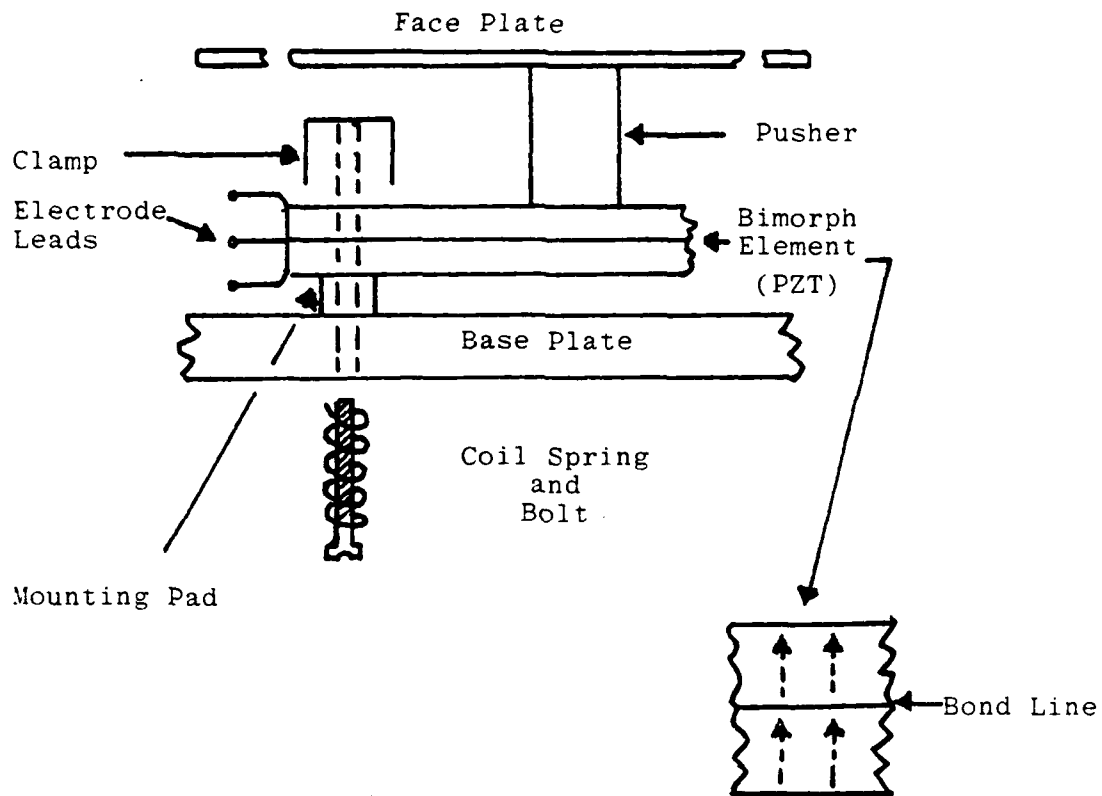
(Polarization state of bimorph elements)

Figure 7 - Bimorph device: Schematic showing actuator
construction and polarization of bimorph

TABLE 4. BIMORPH ACTUATOR: CONSTRUCTION DATA

Number of actuators: 9

Size of bimorph: 3.49 cm X 0.97 cm

Thickness of bimorph: 0.28 cm

Pusher: Stainless steel
         Diameter: 0.97 cm
         Length: 1.27 cm

Adhesive: Armstrong 271 (for pusher-
           bimorph bond)
           Able 849-2 (for bonding
           bimorph plates)

Base plate: Stainless steel

The actual configuration of the bimorph mirror is depicted in Photograph 1.

The mechanical motion of the bimorph element was transferred to the face plate (glass thickness = 0.2 cm) by means of the pusher. The pusher controls the shape of the influence function which is the surface deformation of the face plate.

Figure 7 also indicates the manner in which the bimorph elements are bonded together with respect to the poling direction in each element. The poling direction is the preferential alignment of electric dipoles by means of an external electric field. The two outer surfaces have a voltage polarity opposite the polarity of the interface. Thus, one element contracts while the other expands.

2   Electrical Data

The capacitance and loss tangent values of each bimorph actuator were measured by the usual impedance bridge, described in Appendix C. In comparison with Itek's monolithic piezoelectric mirror (MPM) which has a typical capacitance of 180 pF, the capacitance of the bimorph actuator is considerably greater, with 4 nF as a typical value. The loss tangent of the bimorph is approximately 0.04 which is nearly a factor of four greater than the average loss tangent of the MPM. Of course, the area of a small hole actuator (i.e., the MPM) is considerably less than the area of the bimorph actuator.

3   Dilatational Response

Using a surface profilometer, which is accurate to within 50 Å or 1.0 percent, the measured average deformation was 4.1 μm with a standard deviation of 0.37 μm at ± 1 kV. With an applied voltage of ± 1.5 kV the dilatation increased to ± 7 μm with a standard deviation of 0.46 μm. Greater deformations could have been obtained for a given voltage by using a longer bimorph element to achieve greater bending. However, closely spaced actuators necessitate shorter bending elements.
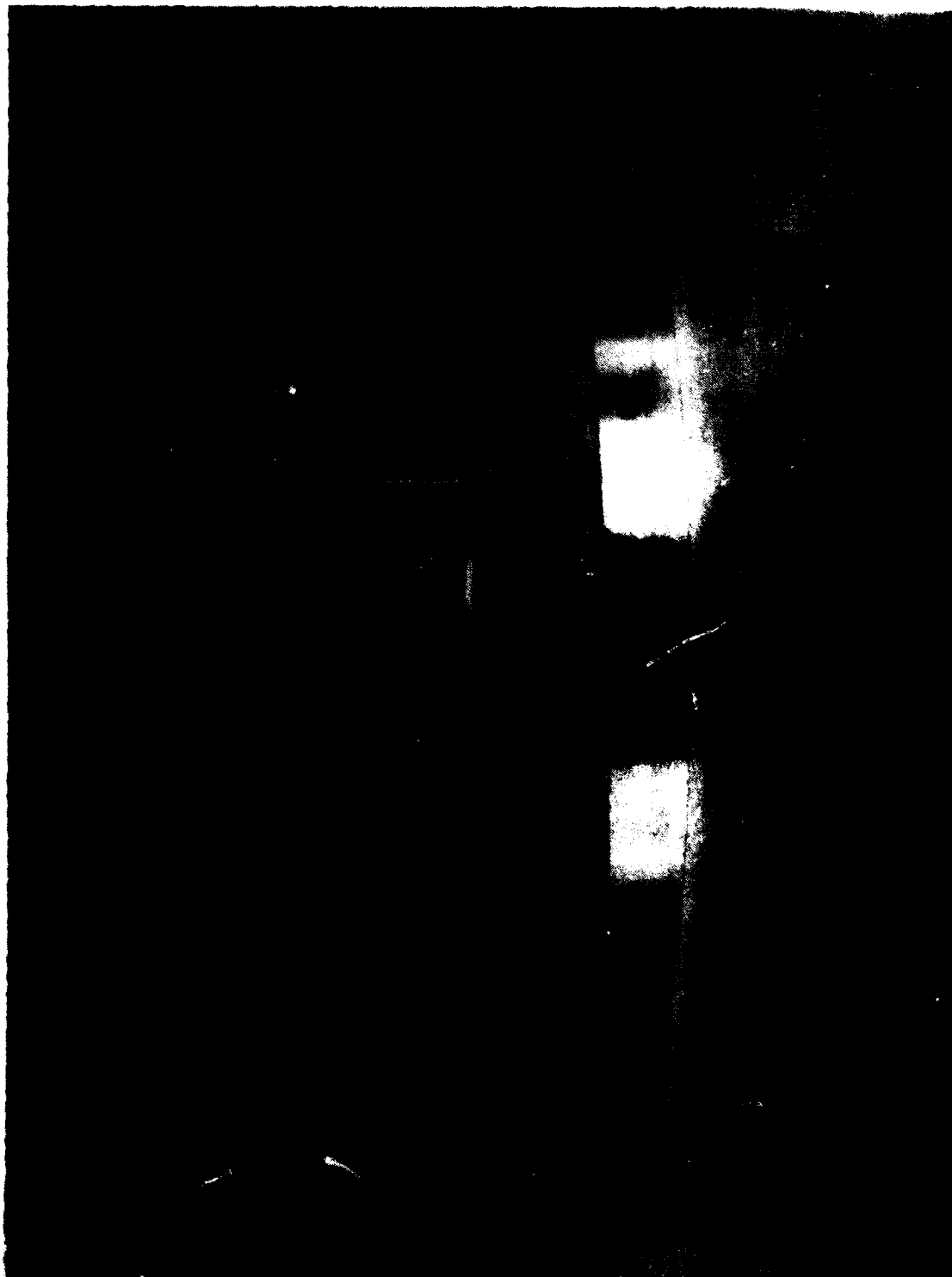
Photograph 1. Bimorph Actuator Mirror

Presented in Figure 8 are two influence functions, one due to +1.5 kV and the other from 1kV applied to an actuator. Observe that the influence function overlap at the adjacent actuator at a distance of 2.54 cm is a sizeable fraction of the function maximum. This overlap could be reduced through proper choice of actuator spacing and face plate thickness, if desired.

Figure 9 is a plot of deformation versus applied voltage for the central actuator. This curve is non-linear in its entirety.

4   Mechanical Resonances

The bimorph device was examined for mechanical resonances by means of electrical techniques which are discussed in Appendix A. This section describes the results of the of the electrical measurement. Figure 10 displays the resonance spectrum obtained by driving the center actuator with a sinusoidal voltage of 100 volts p-p. The frequency of the voltage was varied manually over a range of 100 to 10,000 Hz. No mechanical resonances were detected below 3000 Hz. For this bimorph device the principal resonance activity is concentrated within the 3000 - 7000 Hz band. The concentration of resonance activity in the 0 - 10,000 Hz band is unlike the resonance behavior of the coherent stack-actuator deformable mirror. The reason for this difference is not well understood.

5   Life Test

The bimorph device was subjected to life testing to determine the extent, if any, that the surface figure changes. Using a voltage of ± 750 V at 60 Hz, the device was exercised in a checkerboard pattern for several hours. A summary of the life test is listed below:

23

● = 1.5 kV scan from actuator #5 to #6

X = 1.0 kV scan from actuator #5 to #6
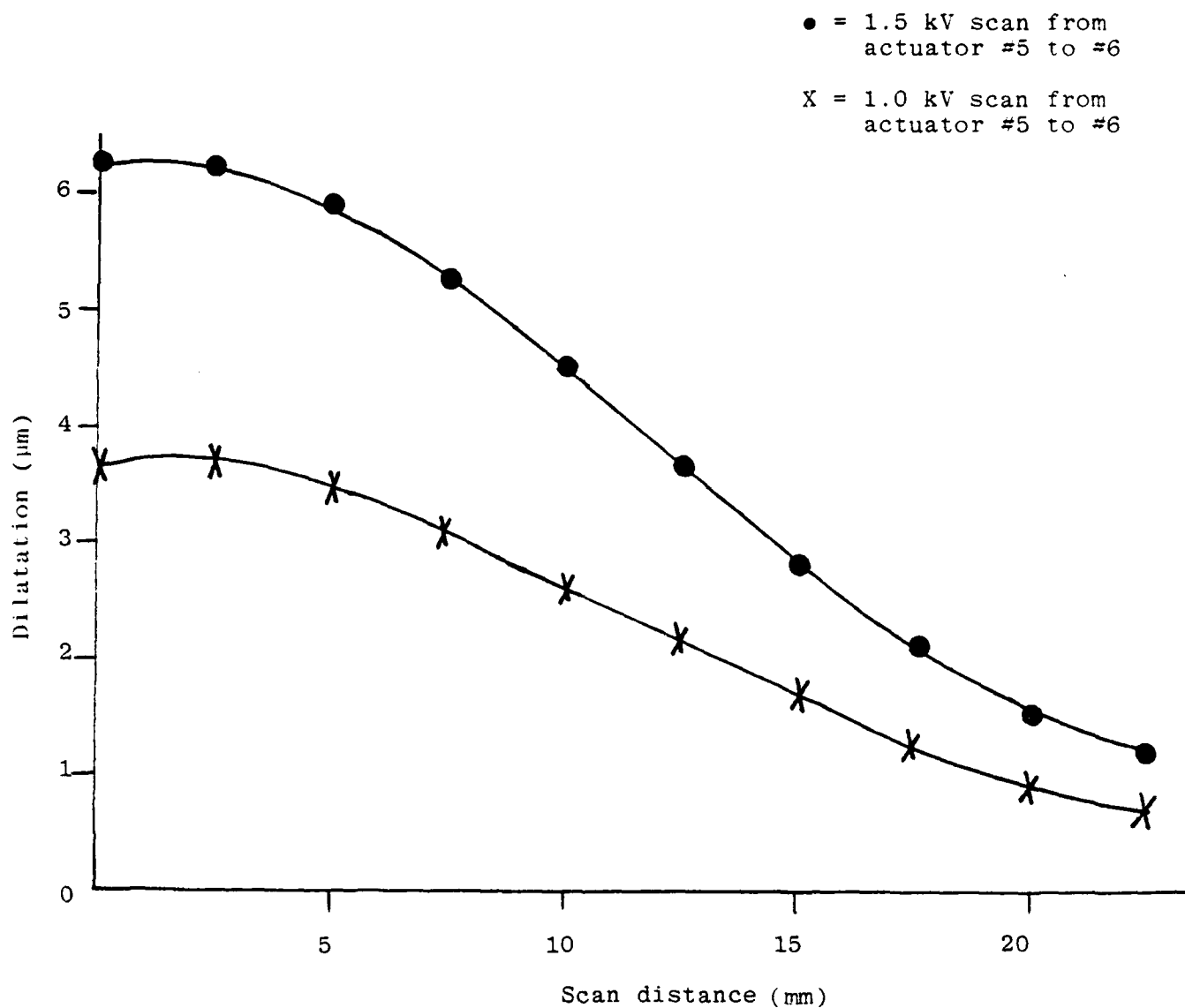
Figure 8 – Bimorph device: Influence function of a bimorph device
which has a glass face plate 0.20 cm thick

24
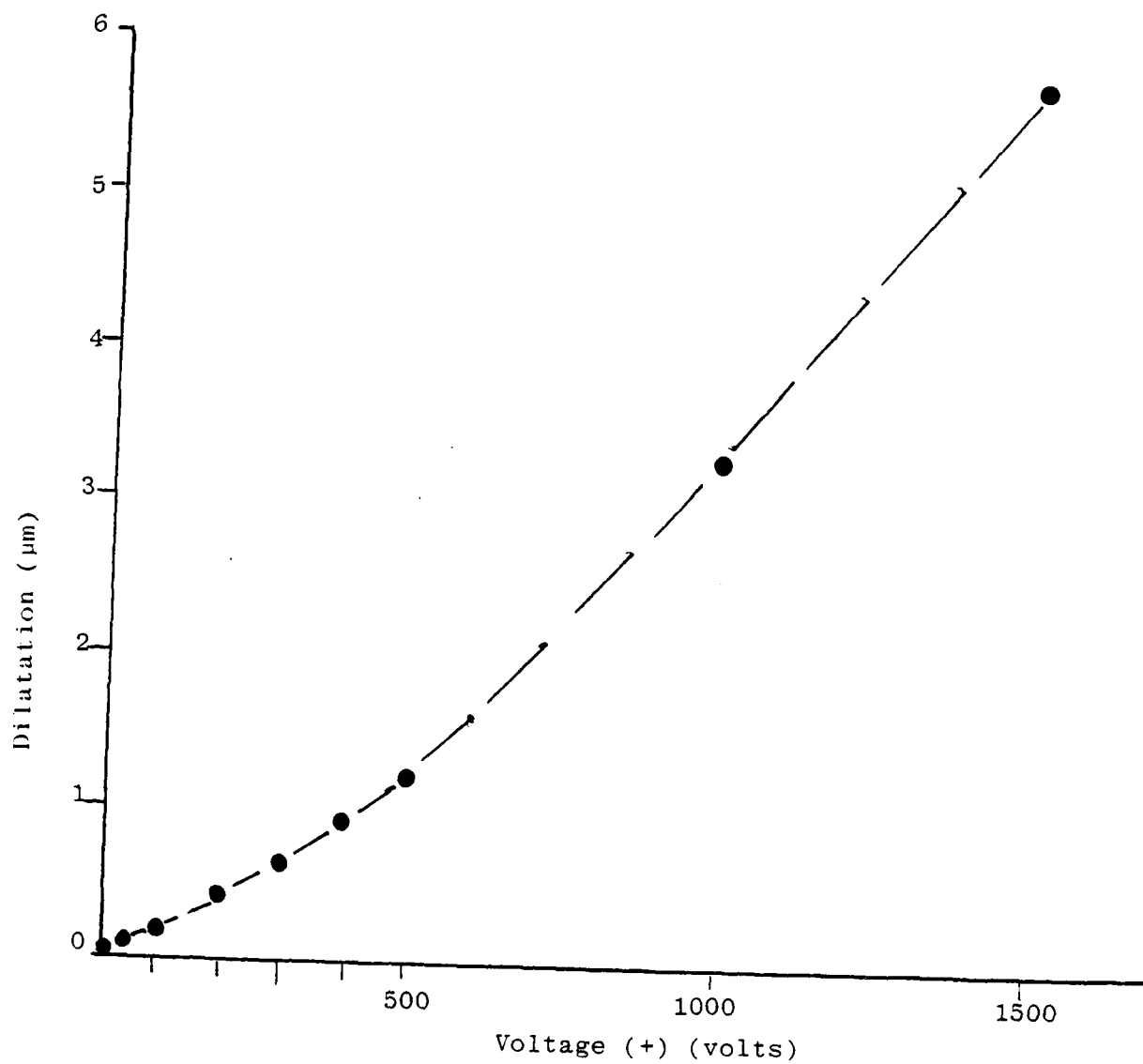
Figure 9 - Bimorph device: Dilatation versus applied voltage
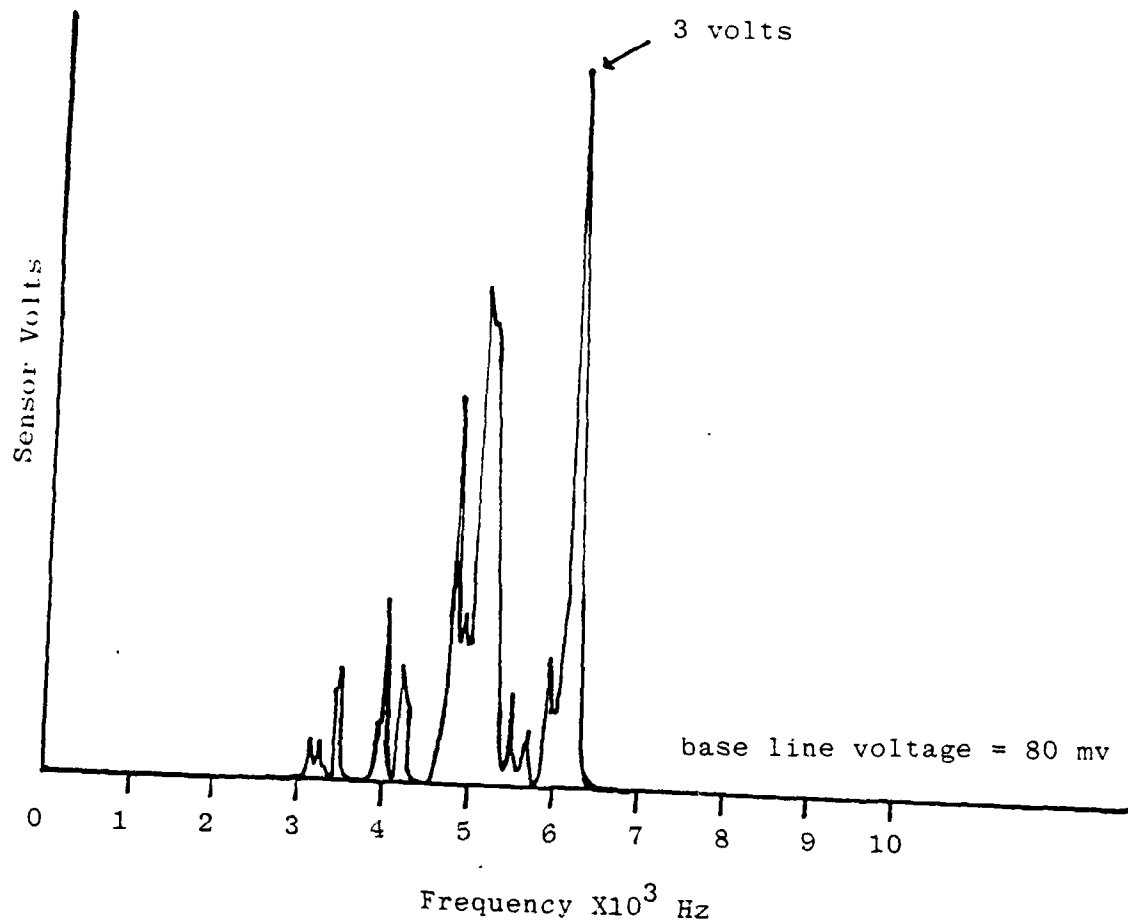
Figure 10 - Bimorph device: Resonance spectrum (voltage change versus driver frequency)

Time	Condition
0 hrs.	80 nm (surface bump)
96 hrs.	40 nm (surface bump)
324 hrs.	160 nm (surface bump)

The surface bump of 80 nm represents the surface figure at the start of the life test. Continued exercising of the device caused this bump to change and is so indicated above. After 324 hours elapsed, the wavefront change amounted to 0.25 λ, where λ is 633 nm. These results indicated that the long term stability of the bimorph device is suitable for the mid-infrared range of 2 - 5 μm and performs surprisingly well in the visible wavelength range.

VI   TUBULAR ACTUATOR

During the program tubular actuators were examined.
Operation of the tube depends upon a transverse piezoelectric
coefficient, whereby the deformation is orthogonal to the
voltage applied across the tube's wall. Hence the "mechanical
advantage" is a function of the tube's length to wall thickness
ratio. A typical tubular actuator is depicted in Figure 11.
Notice that the tube is embedded in the base for stability.
Summarized in Table 5 are the construction details for the
deformable surface device (#162), which employs an array of
9 tubular actuators on 2.54 cm centers.

1   Electrical Properties

Selected actuators were measured for capacitance and loss
tangent using the same apparatus described in Appendix C. The
average capacitance is approximately 6 nF with a loss tangent
of 0.002. The capacitance measurement had a large standard
deviation similar to that observed for the coherent stack
actuator (see Section VII, Subsection 1). However, both the tubular
and coherent stack actuators displayed relatively small standard
deviations for the sensitivity data.

2   Dilatational Measurements

Surface deformation measurements were made by means of a
surface profilometer, which was positioned above each actuator
for sensitivity measurements and then used in a scan mode to
determine the influence function. The latter function is the
surface deformation resulting from one energized actuator.

Figure 12 is a plot of the influence function of the central
actuator (i.e., the fifth one of an array of nine actuators).
The shape of the influence function is, of course, determined
partially by the pusher (see Figure 17 for design details).
However, the influence function for the tube becomes negative
beyond 2.54 cm as seen in Figure 12. This result can be altered

28
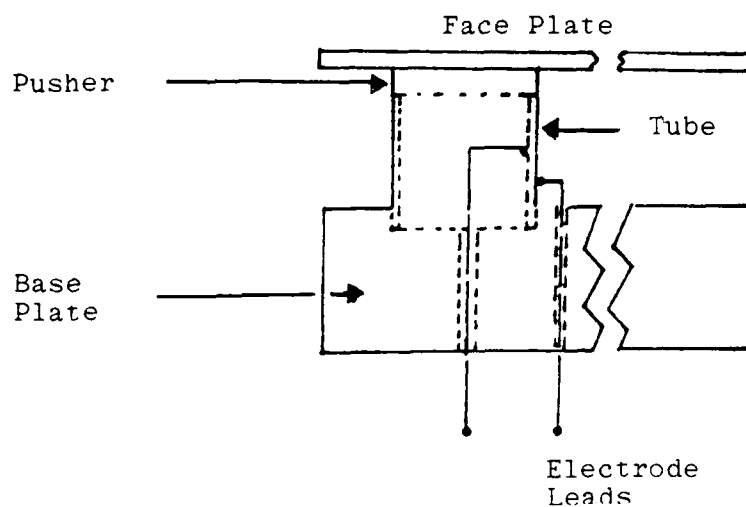
Figure 11 - Tubular actuator construction (#162)

TABLE 5.   TUBULAR ACTUATOR (#162):   CONSTRUCTION DATA

Material: C-5800

Diameter: O.D. 1.27 cm
           I.D. 0.97 cm

Length: 5.08 cm

Number of Actuators: 9

Glass Faceplate: 0.18 cm thickness

Spacing Between Actuators: 2.54 cm

Actuator Pusher: (See Figure 17)

Epoxy: Able (849-2)
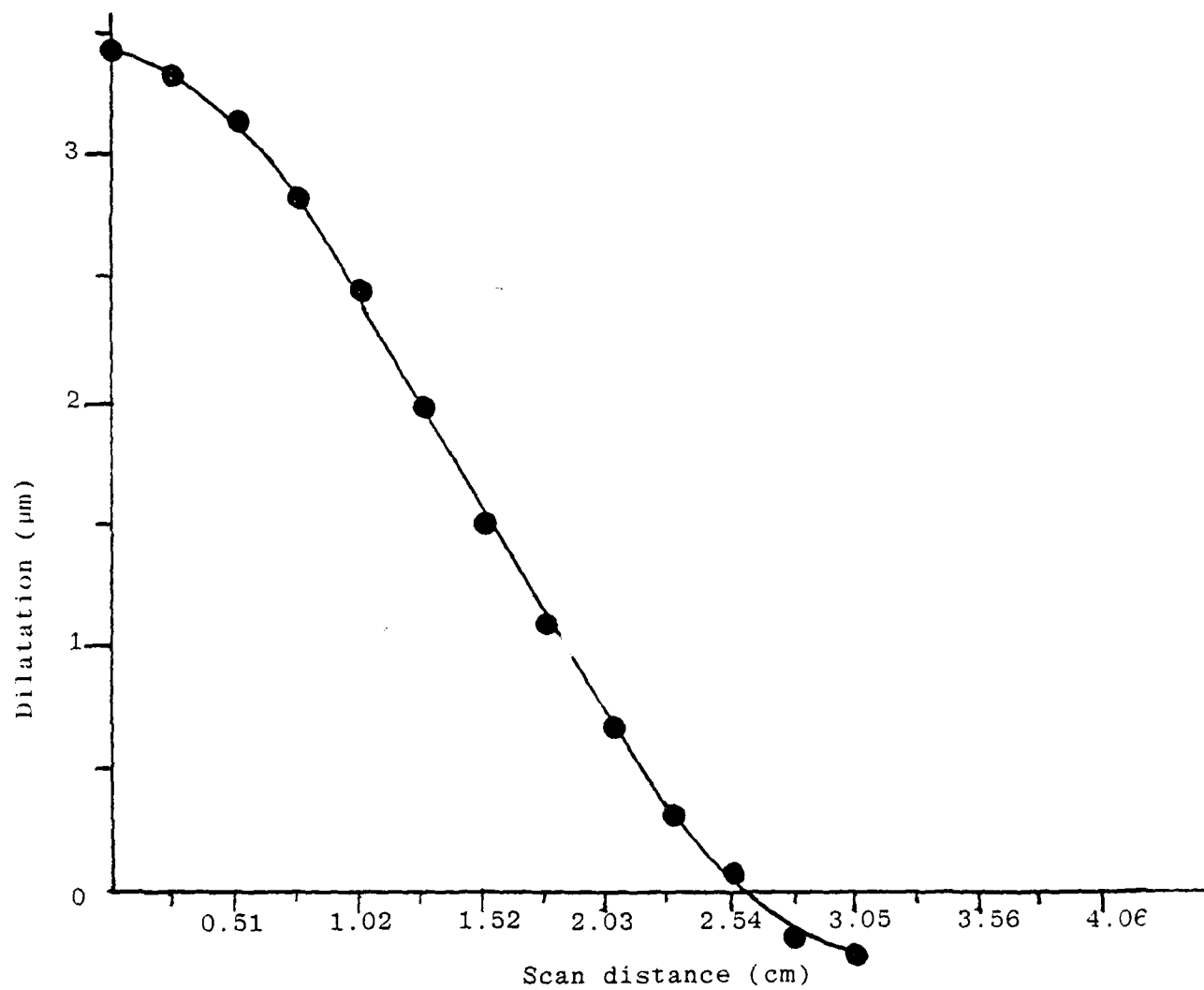
Figure 12 - Tubular actuator (#162): Influence function.
            Applied voltage is +1 kV

30

by varying parameters such as faceplate thickness, actuator spacing, pusher design, etc.

Sensitivity measurements were made for all nine actuators. The average sensitivity is 3.16 μm for an applied voltage of + 1 kV. Consistent with the small sensitivity data range of the coherent stack actuators, the standard deviation of the tubular actuator sensitivity was calculated to be 0.08 μm at + 1 kV (see Section VII, Subsection 2).

Figure 13 shows a linearity test for a sample actuator as a function of applied voltage. Note that the best fit straight line would cross the abscissa at a value greater than zero indicating an increase of sensitivity with applied voltage at least in the range of 0 to 1000 volts. The data also shows that a dilatation of nearly 6 μm was achieved at + 1.5 kV.

3   Temperature Data

Device #162 was placed in an interferometer and heated 10°C above ambient and allowed to cool. Similarly the same device was later cooled 10°C below ambient and allowed to warm at room temperature. During both cycles interferograms were taken to show the change, if any, in the surface figure. The results of these measurements are provided in Figure 14, which shows the changes in fringes as a function of temperature. The pusher used for the tubular actuator (see Figure 17) was thought to allow a sufficient amount of flexure to accommodate temperature stresses. The behavior exhibited in Figure 14 is typical of several coherent stack actuators, which were subjected to the same type of temperature test. Our conclusions, discussed at greater length in Subsection 3 of Section VII, indicate that temperature invariance (i.e., athermalization) is best achieved by matching the temperature expansion coefficients (i.e., use of the same material for the face plate and the pusher) and sparing, careful use of epoxy.
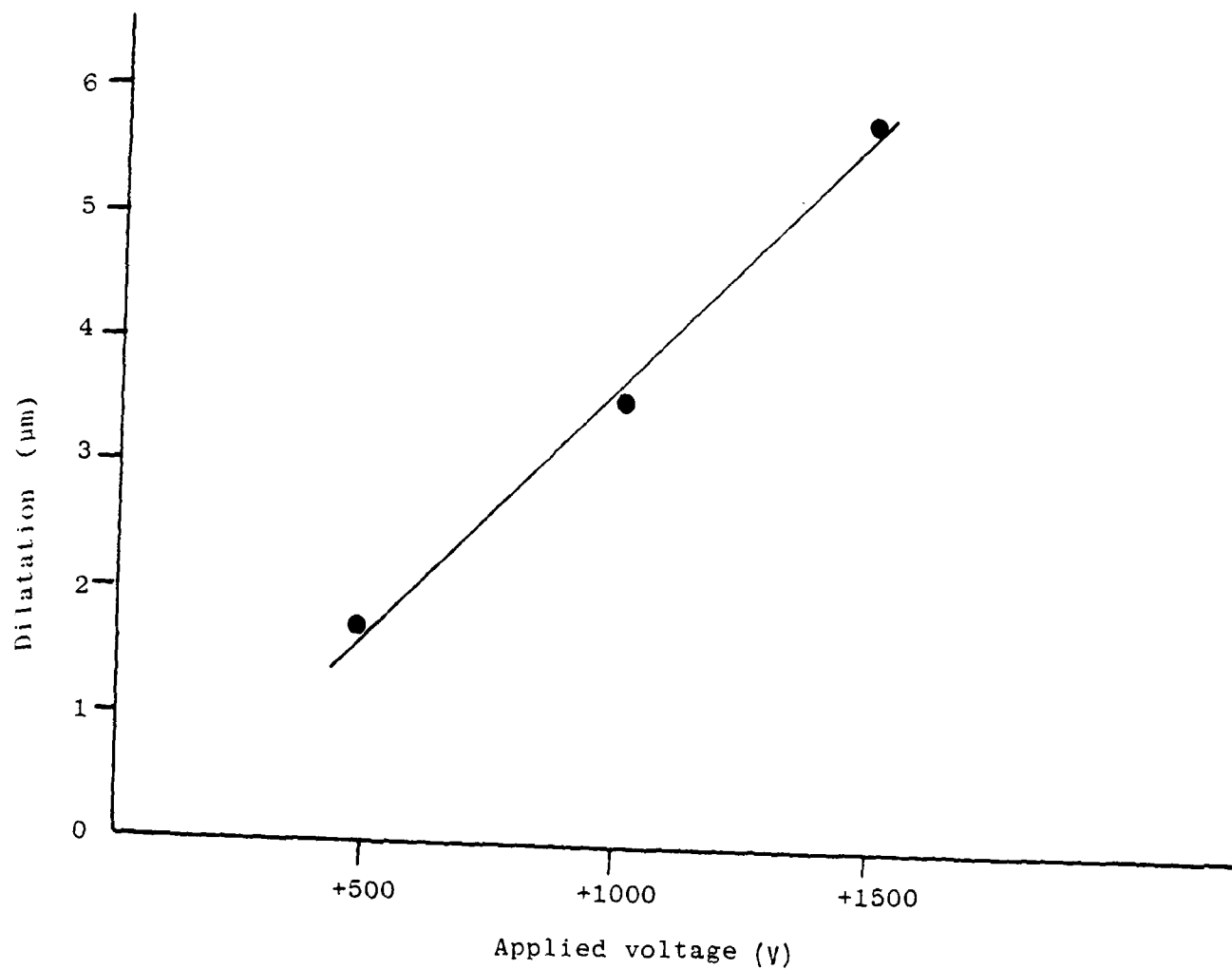
Figure 13 - Tubular actuator (#162):   Dilatation versus
applied voltage

32
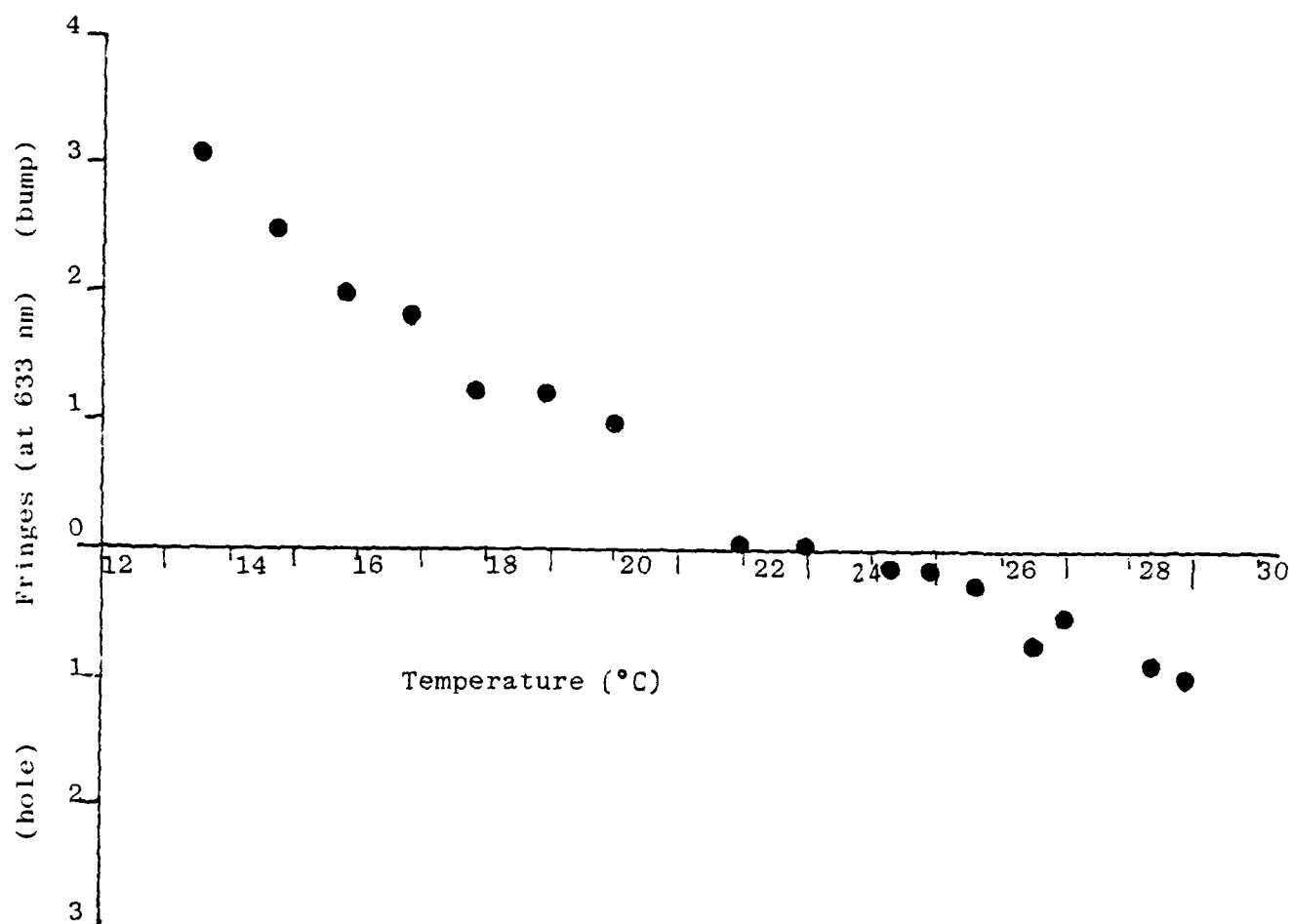
Figure 14 - Tubular actuator (#162): Change of surface figure
with temperature

4   Mechanical Resonances

The tubular actuator device was examined for mechanical resonances by both optical and electrical measurement techniques.   See Appendix A for a brief description of these procedures.

Shown in Figure 15 is the resonance spectrum of device #162, whose central actuator was driven at 100 volts (peak-to-peak) and over a frequency range of 0.2 to 15 kHz.   The first resonance occurred at a frequency of about 2.3 kHz and is presumably the fundamental drum-head mode.   Beyond 6.5 kHz the resonance pattern increases and becomes significantly more intense and broad band beyond 8 kHz.   These results are typical of the coherent stack resonance pattern when the same pusher (see Figure 17) was employed with the stack.   Apparently this pusher, originally conceived as a means of temperature stress accommodation, allows flexibility during resonance by offering less clamping.   Clamping almost always shifts the resonant frequencies to greater frequency values.

34
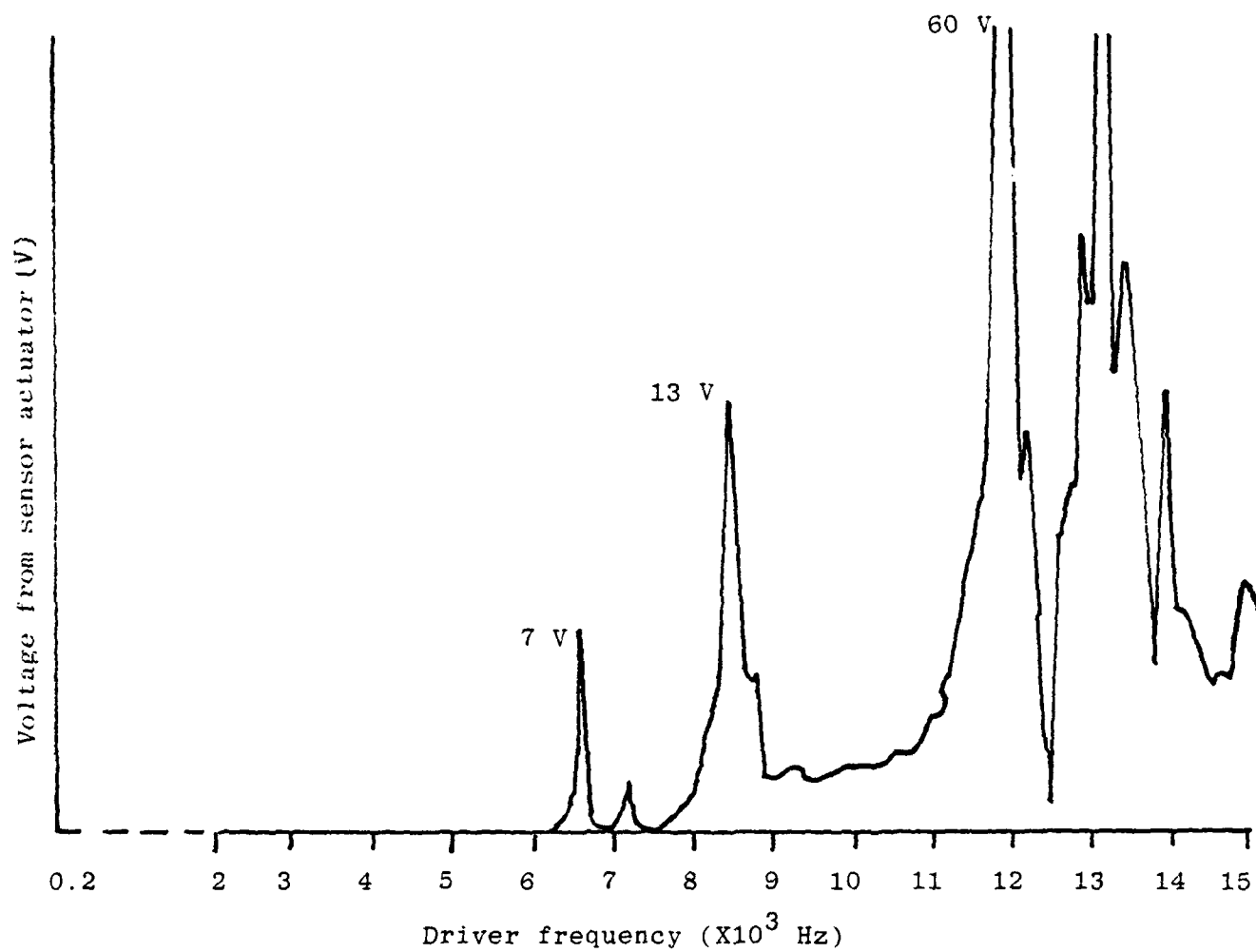
Figure 15 - Tubular actuator (#162): Resonance curve (voltage change
versus drive frequency)

35

VII COHERENT STACK DEVICES

Several coherent stack devices were fabricated and
tested to determine the viability of this actuator type
in terms of program goals. Depicted in Figure 16 is a
typical coherent stack, which is constructed from PZT discs
bonded with epoxy and then sliced into an actuator array
before making electrical contacts. This method of construc-
tion affords structural uniformity in that the Xth layer of
all actuators has similar properties (i.e., similar in
ceramic characteristics) because this particular layer in
each actuator was cut from the same disc.

Given in Table 6 are the construction details of the
coherent stack devices, together with the data concerning
the pushers. Following Table 6 is a photograph of a coherent
stack device (#160) which has 21 actuators. Situated between the
glass face plate and the actuators, the pushers are responsible
for controlling the shape of the influence function. Several
pusher designs and materials were examined to insure that the
surface optical figure remains unaffected by temperature
changes. One particular novel pusher design, illustrated in
Figure 17, was utilized for its athermalization properties.

1   Electrical Measurements

Listed in Table 7 are average values of capacitance and
loss tangent for four coherent stack devices. These values
were computed from measurements made by an impedance bridge,
discussed in Appendix C. The average capacitance of the
devices, ranging from 7 nF to nearly 9.5 nF, has a somewhat
large standard deviation (σ). For example, there is a range
of 4.28 nF to 9.78 nF for device #158. As a point of reference,
Itek's monolithic piezoelectric mirror (MPM) exhibits a typical
capacitance of about 180 pF with a standard deviation of nearly
10 pF. There is, however, a considerable difference in actuator
surface area between an MPM and a coherent stack.
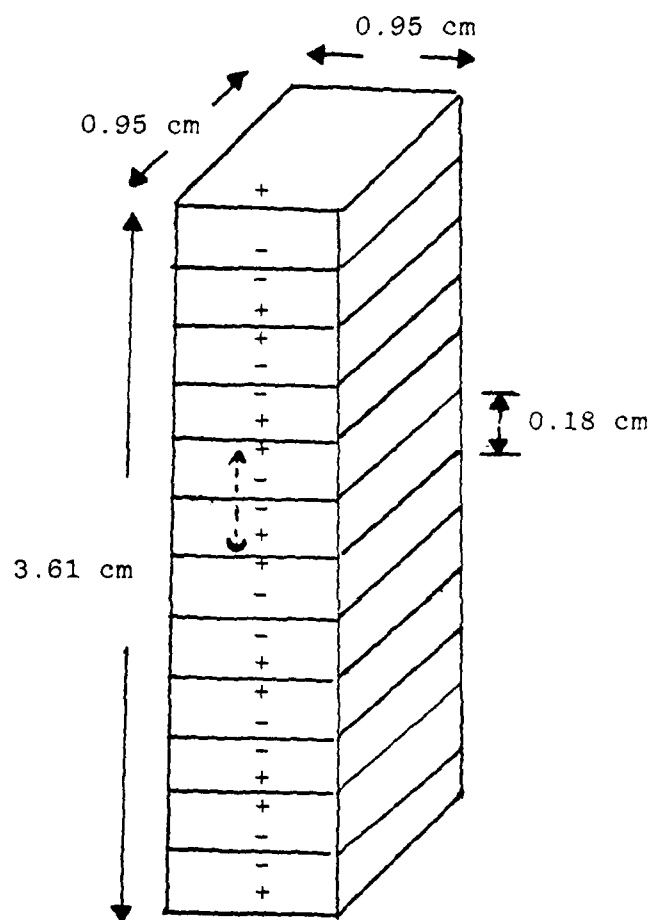
Number of layers in stack	20
Center-to-center actuator spacing	2.5 cm
Actuator mounting (baseplate)	Glass (1.27 cm thick)
Actuator pusher (stainless steel)	Diameter = 0.64 cm
	Height = 0.32 cm

Figure 16 - Typical construction and data for actuator stack. The
dotted arrows indicate polarization of the ceramic layer

TABLE 6.   COHERENT STACKS: CONSTRUCTION DATA

Number of Layers in Stack   20 (except for #160, which has 21)

Layer Dimensions   0.18 cm thick, 0.95 cm square
                                 (see Figure 16)

PZT Material   Channel 5800 (low hysteresis)

Epoxy   Abelbond 849-2 (copper doped) all
                                 joints

Center-Center Actuator
   Spacing   2.5 cm

Actuator Mounting   "Macor" machinable glass (1.27 cm
                                 thick

Actuator Pusher   Diameter   Height   Material

   Device #158   0.64 cm   0.32 cm   Stainless steel (416)
   Device #160   0.56 cm   0.23 cm   Stainless steel (416)
   Device #161   (See Figure 17)
   Device #164   0.64 cm   0.32 cm   Glass (7740)

Photograph 2.   Coherent Stack Actuator Mirror

38
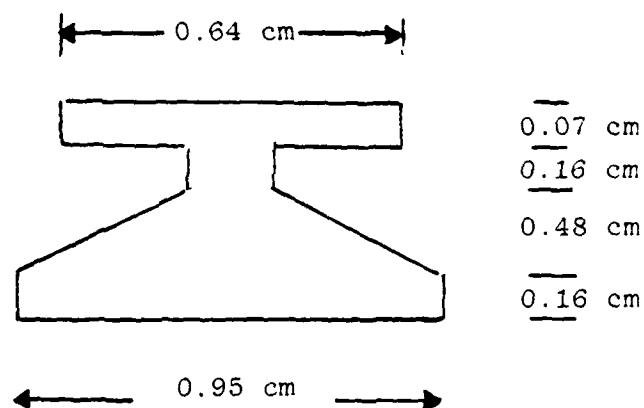
Figure 17 - Coherent stack: Pusher dimensions for actuators of
         device #161. Pushers are machined from stainless
         steel (416)

TABLE 7. COHERENT STACK DEVICE: MEASURED ELECTRICAL
          PROPERTIES

Device Number	Capacitance (nF)		Loss Tangent	
	Average	σ*	(average)	σ
158 (9 actuators)	7.84	1.94	0.14	0.20
160 (21 actuators)	9.48	1.27	0.03	0.02
161 (9 actuators)	7.09	1.38	0.03	0.03
164 (9 actuators)	9.02	1.38	0.03	0.06

*σ = standard deviation

2   Dilatational Properties

Given in Table 8 are the dilatational responses of
four coherent stack devices, whose actuators were subjected
to 1500 volts. The amount of surface deformation was measured
with a surface profilometer (DekTak), which has a measurement
capability to within 50 Å or 1 percent. Once again average values and their
respective standard deviations are quoted. A glance at Tables
7 and 8 reveals that there is less spread in the sensitivity
data than in the electrical data. This result indicates that
the dilatational response is less sensitive to the details of
actuator construction and variation in materials (i.e., the
piezoelectric ceramic and epoxy bond). Tables 7 and 8 also
suggest that the devices with higher sensitivity tend to have
higher capacitances. Numerous different devices built at Itek
tend to confirm this observation.

Further dilatational measurements were conducted to determine
linearity of actuator response. Voltages of 500, 1000 and 1500
were applied to the central actuator of the devices listed in
Table 9. Using the data from device #158 as a typical example,
Figure 18 illustrates the behavior of coherent stack
devices, at least within the limit of voltages used during the
measurement.

The influence function was also measured by means of the
same profilometer, but employed in a scan mode. By definition,
the influence function is the amount of surface deformation
which extends radially from an energized actuator. Figure 19
depicts a typical influence function, which is approximately
gaussian in form. The figure also shows that this function
becomes zero at the adjacent (unenergized) actuator.

The amount of response at the adjacent actuator is frequently
referred to as meshing, which as a percent of the maximum
dilatation, ranges from 0 to 3 percent for the coherent stack
type actuators. This amount of meshing is desirable in terms

TABLE 8.   COHERENT STACK DEVICES: MEASURED SENSITIVITY
DATA

Device Number	Dilatation (μm/+1.5 kV)		Meshing (%)	Glass Face Plate	
	Average	σ*		thickness (cm)	diameter (cm)
158 (9 actuators)	7.37	0.55	0	0.20	10.16
160 (21 actuators)	7.85	0.17	3	0.23	15.24
161 (9 actuators)	7.44	0.11	0	0.18	10.16
164 (9 actuators)	8.00	0.13	0	0.17	10.16

*σ = standard deviation

TABLE 9.   COHERENT STACK DEVICES: MEASURED SURFACE
DILATATION AT SELECTED VOLTAGES TO TEST FOR
LINEARITY

Device Number	Glass Thickness (cm)	Dilatation (μm)			Actuator Number
		(+500V)	(+1000V)	(+1500V)	
158	0.20	2.68	5.40	8.40	5
160	0.23	2.55	5.20	8.10	11
161	0.18	2.48	5.00	7.90	5
164	0.17	2.70	5.60	8.60	5
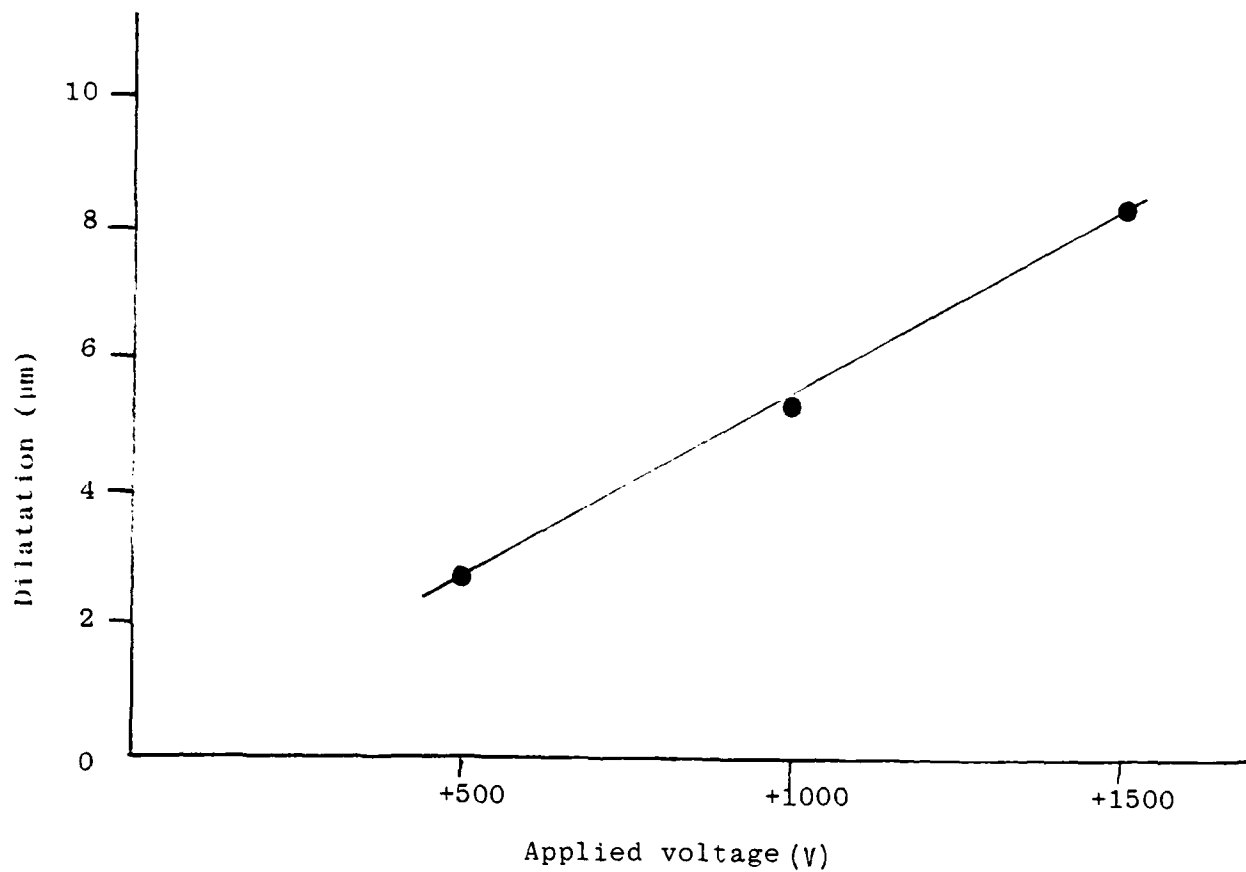
Figure 18 - Coherent stack device (#158): Dilatation versus
applied voltage
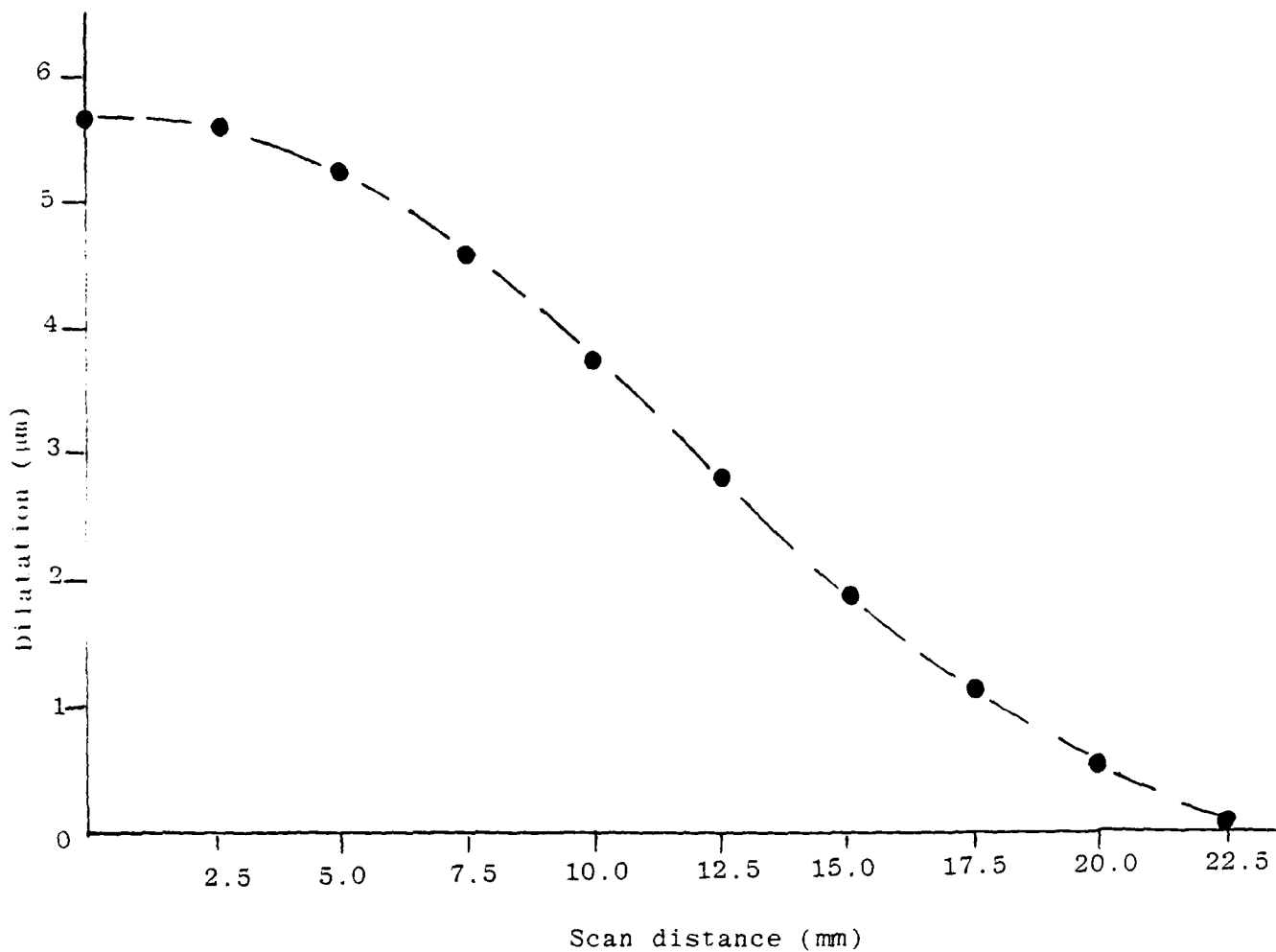
Figure 19 – Coherent stack device (#158): Influence function of actuator #5 (profilometer scan made between actuators #5 and #6)

of the algorithm employed for wavefront correction. That is, too much meshing generates "cross talk" between actuators and must be subtracted, while too little meshing causes residual ripple in the "corrected wavefront".

3   Temperature Data

The athermalization of the coherent stack device with respect to ambient changes has been examined with particular emphasis on the faceplate/pusher interface. Pushers, made from stainless steel, Invar (approximately 36 At % Ni) and glass, were bonded to glass faceplates. Most of these pushers were cylindrically shaped except for some made from stainless steel in the form of a thin flat disc which "necked down" to a base region (see Figure 17). It was thought that this shape would better accommodate flexural changes encountered during thermal cycling.

These components were placed in an interferometer and heated approximately $10^{\circ}C$ above ambient and allowed to cool. Temperature was measured by a thermocouple. Interferograms were taken periodically during the cooling cycle and later measured to determine changes, if any, in the optical figure. The same process was repeated after cooling the device about $10^{\circ}C$ below ambient. The result of this procedure is illustrated in Figure 20 for device #158, which employs stainless steel pushers.

Various pusher designs and materials were examined and are summarized in Table 10. Invar-36 has a coefficient of thermal expansion (α) nearly that of the glass faceplate. For example, α (Pyrex) is $3.29 \times 10^{-6}/^{\circ}C$ while α (Invar-36) is about $2.70 \times 10^{-6}/^{\circ}C$. This amount of thermal coefficient mismatch was sufficient to cause about 3 fringes of shift (at 633 nm) with the presence of the epoxy fillet. The fillet is the excess of epoxy around the edge of the pusher-to-faceplate interface. Removal of the fillet resulted in slightly improved performance

44
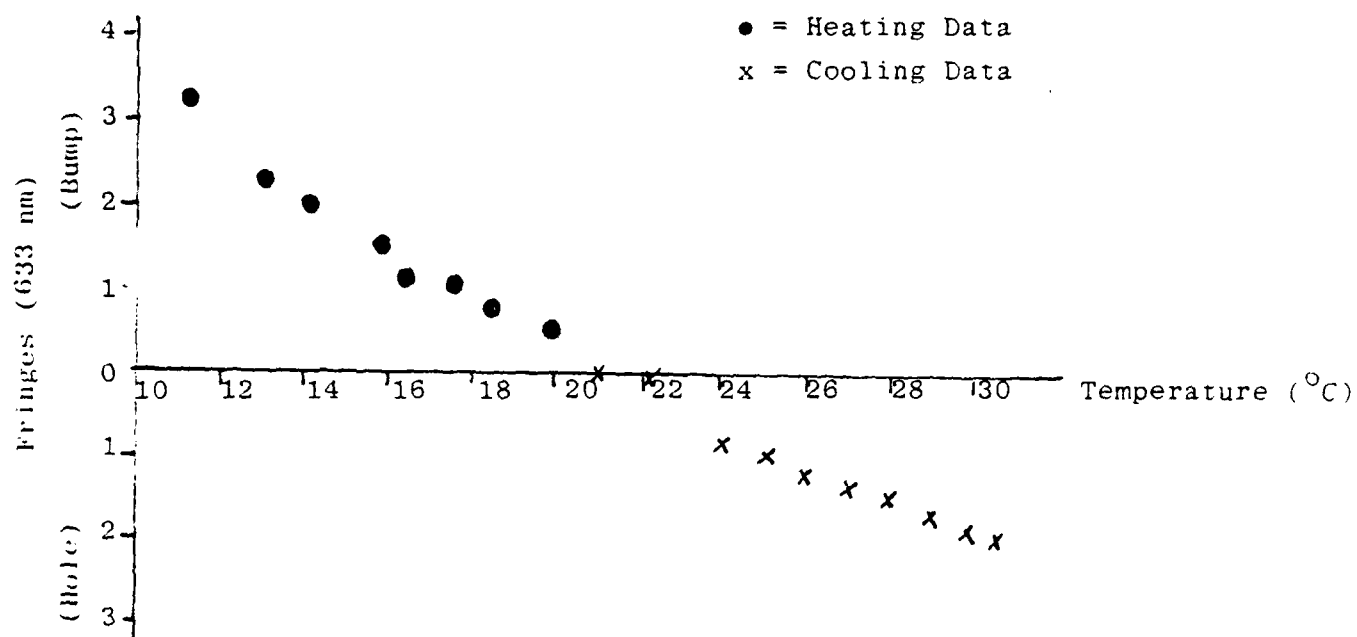
Figure 20 - Coherent stack device (#158):   Interferometric
            measurement of optical figure change as a function
            of temperature

with a change of only two fringes.

The data in Table 10 show that the stainless steel pusher of the "neckdown" type performed in nearly the same fashion as the Invar cylinder type. Apparently, the flexure design itself provided some improved thermal stability in view of the fact that α (stainless 416) is $17.82 \times 10^{-6}/{}^{\circ}C$.

The performance of glass pushers with fillets is nearly equal to the previous two cases. However, fillet removal causes an enormous improvement in surface figure stability over the cycled temperature range. It should be noted that before thermal cycling removal of the epoxy fillet at the edge of the face plate/pusher interface caused a surface indentation of approximately 3 fringes in the vicinity of the actuator. This dip may be removed simply by polishing.

The explanation for the existence of the dip in the surface begins with the initial bonding. After curing the epoxy at an elevated temperature the epoxy bond undergoes greater shrinkage than does the glass. Hence the surface bows out. The surface is subsequently polished to remove the bowed-out areas. Removing the epoxy fillet causes the surface to bow in the opposite direction.

The above experiments suggest that optical figure stability can be preserved in the presence of thermal fluctuations by maintaining a thin bond line, removing fillets and matching expansion coefficients of pusher and face plate. To the extent of our current series of measurements, the fillet at the pusher/actuator interface does not contribute to thermal instability.

In addition to the invariance of figure stability in the presence of external temperature fluctuations, coherent stacks have been further characterized by measuring figure change due to actuator heating. By driving the actuators with greater

TABLE 10. COHERENT STACK DEVICE: ATHERMALIZATION DATA

| Pusher | | Bonding | Fringe Change 10°C Above |
Material	Shape	With/Without Fillet	and Below Ambient
Invar	Cylinder	With	3 Fringes
S.S.	Cylinder	With	3 Fringes
Stainless Steel	Neck Type Flexure	With	2 Fringes
Stainless Steel	Neck Type Flexure	Without	2 Fringes
Glass	Cylinder	With	2 Fringes
Glass	Cylinder	Without	1/2 Fringe

voltage for longer periods of continuous use, which would not be expected during "real" conditions, we have attempted to find the upper limit in figure change from the actuator itself. Figure 21 indicates the temperature increase by operating an actuator at $\pm$ 1 kV at a frequency of 1 kHz for periods of 1, 3, 5, 10 and 15 minutes. After each period of operation the actuator was allowed to return to ambient, at which time the actuator was driven for a longer period. Figure 21 shows asymptotic behavior between temperature rise and time of operation. Temperature was measured with a thermocouple in the same manner as before.

4   Mechanical Resonances

Several coherent stack devices were examined for resonances, which were measured both electrically and optically. The results of the electrical data are presented in this section. Appendix A provides a brief description of the experimental details for both methods of measurement.

Figures 22, 23 and 24 display the resonant lines for devices #158, 160 and 161, respectively. For each of these devices the central actuator was exercised at 100 volts peak-to-peak. The base line (i.e., off-resonance) voltage, detected at a neighboring actuator (i.e., sensor electrode), was on the order of several millivolts.

Over the frequency range of 1 - 10 kHz only one resonance line at 9500 Hz was recorded by the x-y plotter as shown in Figure 22. On the same figure, however, are listed several other resonant lines, which were measured by an oscilloscope used to monitor the sensor actuator. The reason these were not recorded by the plotter is uncertain at present, but could have been due to a problem with the set-up since the resonances were observed during the test in the raw data.

48
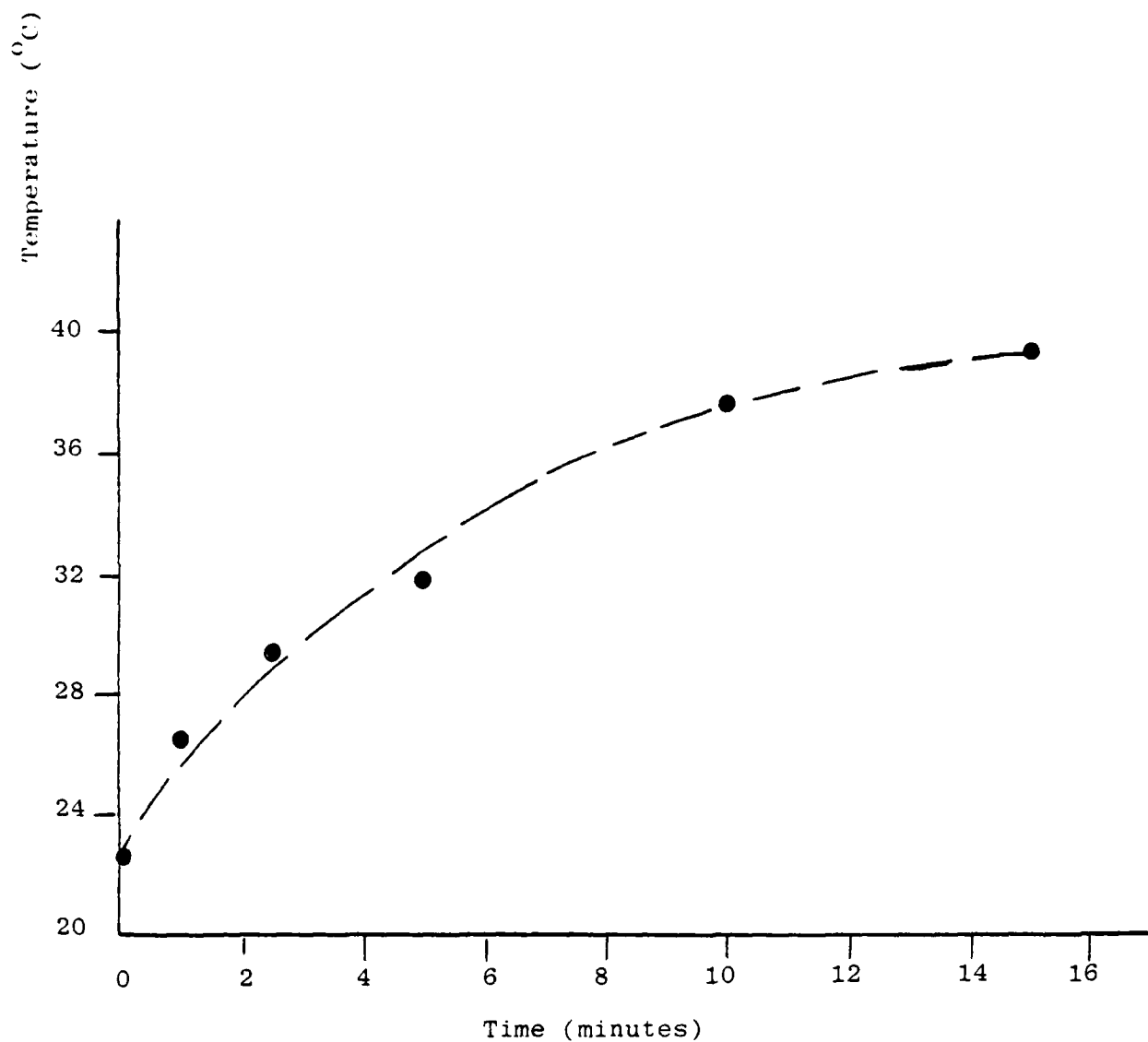
Figure 21 - Coherent stack device (#158):   Actuator heating versus
operation time.   Each data point begins at room temperature

49

Listing of additional resonances measured on oscilloscope.

Frequency (Hz)	Voltage (volts)
2800	0.10
3070	0.45
4900	0.20
5600	0.10
6510	0.33
7090	0.15
7800	0.15
8100	0.15

Figure 22 - Coherent stack device (#158): Resonance curve (voltage change versus driver frequency) for most dominant resonance line
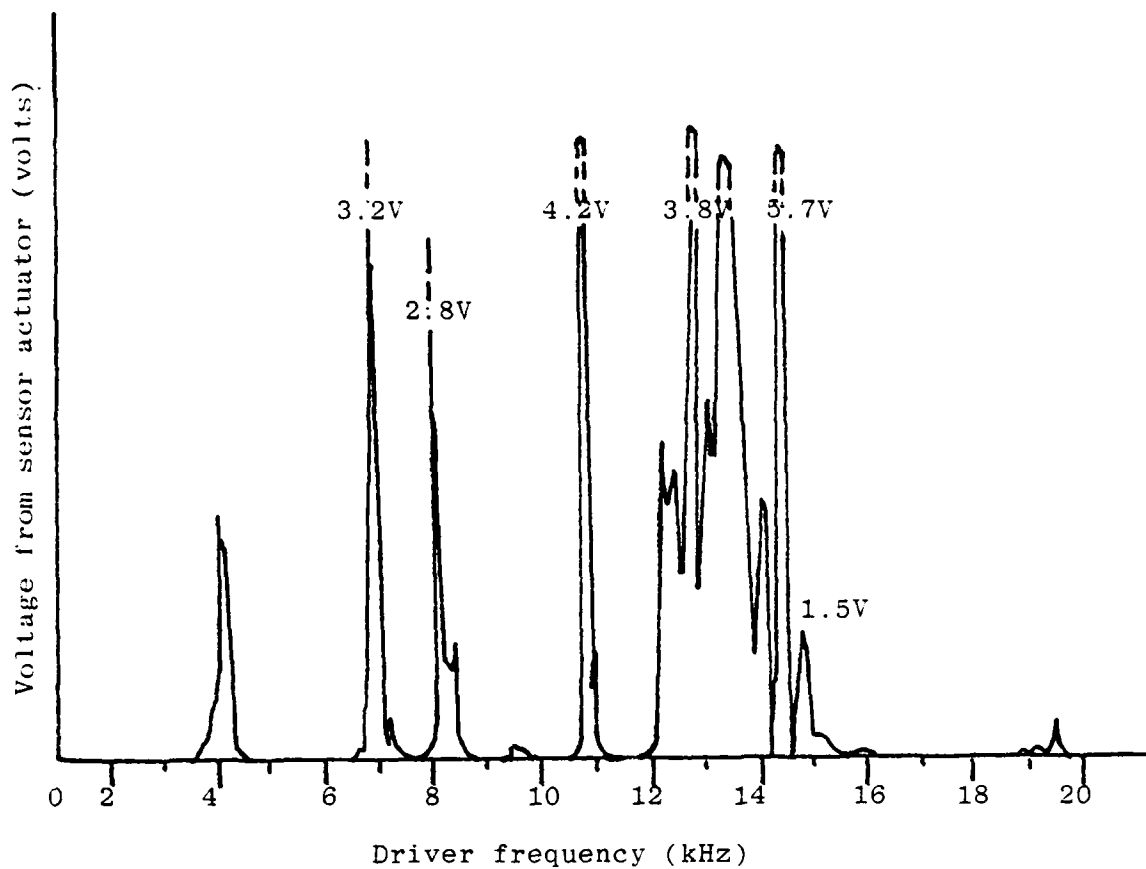
Figure 23 - Coherent stack device (#160): Resonance curve
(voltage change versus driver frequency)

51
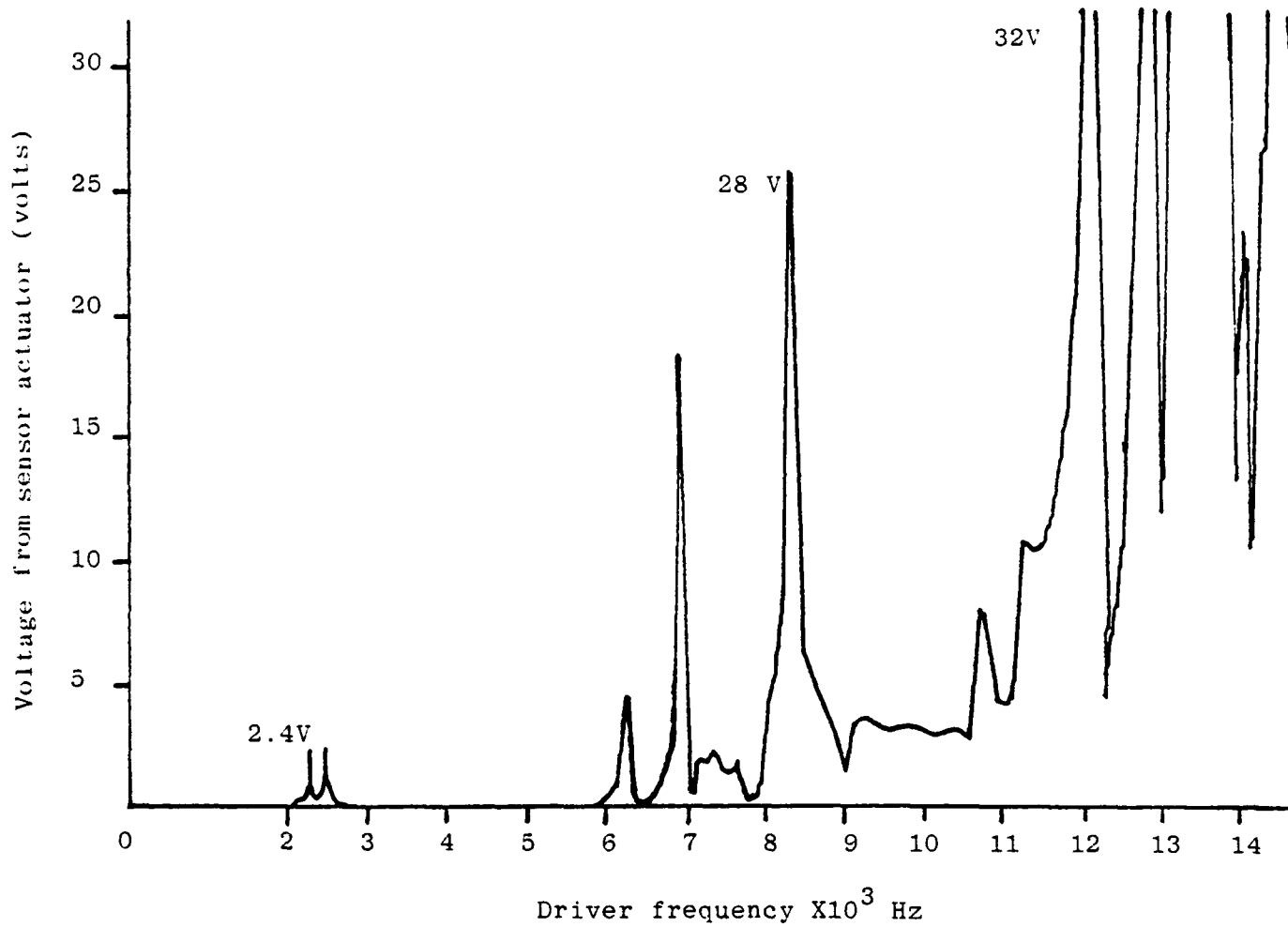
Figure 24 - Coherent stack device (#161): Resonance curve
(voltage change versus driver frequency)

In contrast to the above resonance data of device #158 (a nine actuator mirror) is the resonance spectrum of device #160, which has 21 elements (see Figure 23). There are several sharp resonances in the frequency range of 1 - 10 kHz. These lines have, however, approximately the same magnitude as the one discernible line in Figure 22. Both devices in Figure 22 and 23 employ disc type pushers.

The resonance curve (Figure 24) for device #161 is interesting in that the amount (and also magnitude) of resonance activity has increased beyond the resonance behavior of devices #158 and #160. This result may be attributable to the flexure (see Figure 17) design of device #161. Originally conceived as a means of athermalization, this flexure apparently makes a negative contribution towards the mechanical resonance problem while at the same time providing some benefit in terms of thermal stability.

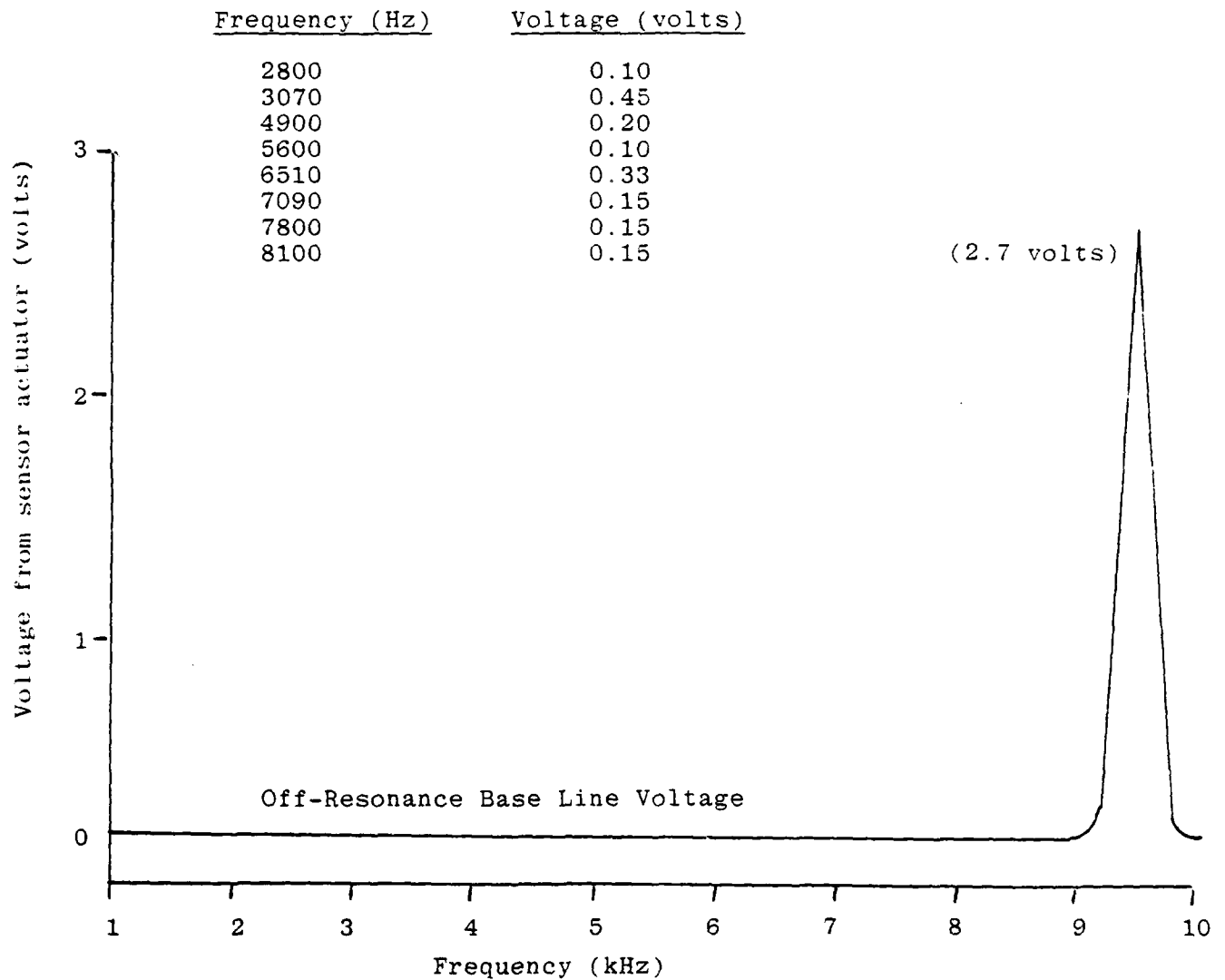In general, the resonance data indicates that the fundamental resonance is above 2 kHz for the type and size coherent stack device considered during this investigation. This result is encouraging since the calculated fundamental resonances for individual component parts (e.g., the face plate and the actuator columns) are considerably less than 2 kHz. Bonding of these components provides a certain degree of clamping which tends to raise the fundamental frequency. The exact analysis of these boundary conditions is somewhat complex and has not been attempted during this program.

5   Life Testing

Device #158 was subjected to life testing for a period of several hundred hours, frequently under conditions thought to be considerably more severe than those conditions encountered during routine use. The test involved exercising adjacent rows of electrodes. Figure 25 shows the initial surface and the condition of the surface after each exercise period. Table 11

A. INITIAL SURFACE.
TEMPERATURE = 21.5°C

B. AFTER 100 HRS. AT 4 μm AND 100 HRS
AT 6 μm, TEMPERATURE = 21.0°C

C. AFTER 100 HRS. EACH AT 4, 6, AND 8 μm,
TEMPERATURE = 21.0°C.

D. AFTER 100 HRS. EACH AT 4, 6, 8, AND 12 μm.
TEMPERATURE = 20.5°C
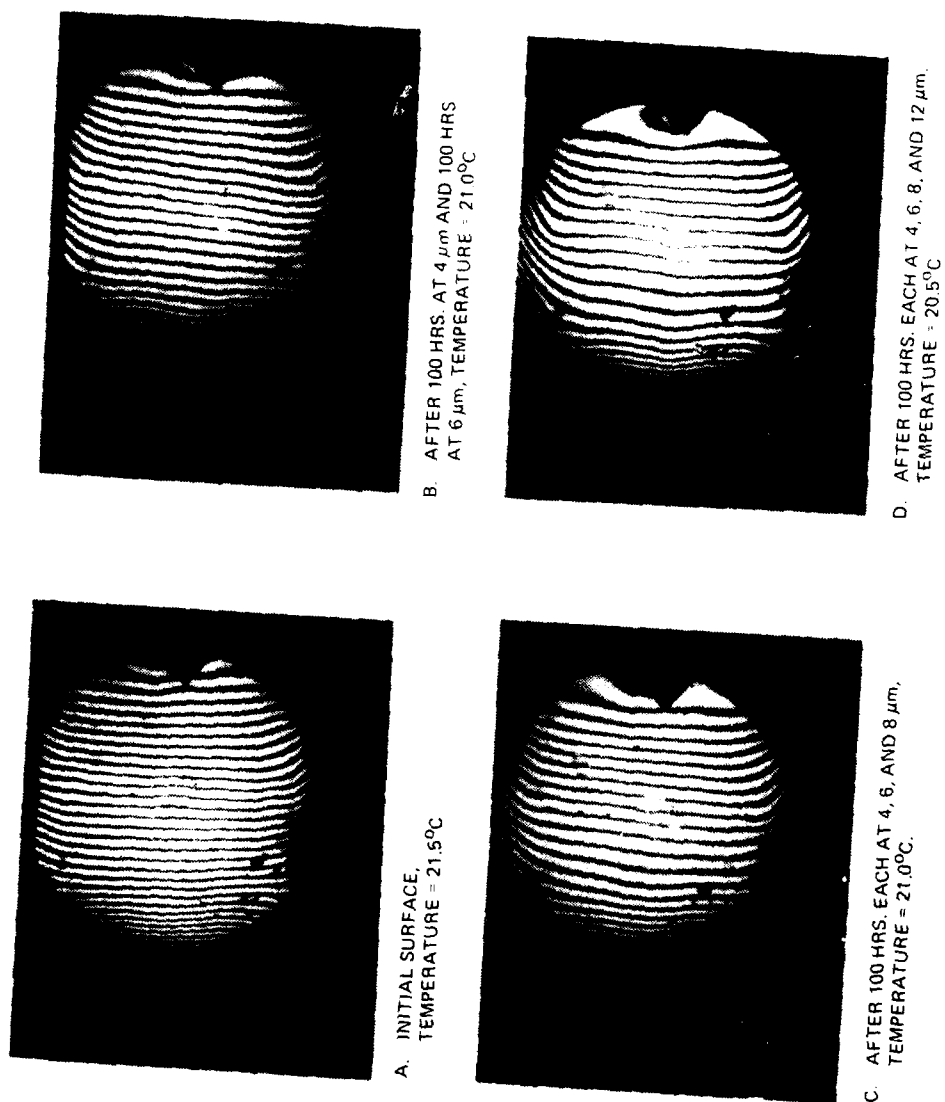
Figure 25.   Interferograms (λ = 0.6328 μm) indicating surface
quality of a coherent stack device after life testing.

TABLE 11.   LIFE TEST RESULTS OF COHERENT STACK ACTUATOR
            MIRROR

Duration of Test (hrs.)	Dilatation (μm)	Result
0 - 100	4	No discernible change
100 - 200	6	No discernible change
200 - 300	8	<0.20 λpp = 63 nm surface deformation
300 - 400	12	<0.36 λpp = 118 nm surface deformation

summarizes these results. Note that the 8 and 12 μm dilatations
are significantly greater than the program goal of 6 μm. Also
of importance is the fact that "footprinting", a change in surface
contour in the vicinity of an actuator, no longer is a problem.
This difficulty, present at the outset of the program, was circum-
vented by use of the copper doped epoxy (Able 849-2).

Additional life testing was undertaken using device #160,
a nine actuator stack mirror. A second layer of glass (0.18
cm thick) was bonded to the face plate (0.23 cm thick). The
sensitivity was then measured to be 6.6 μm/+ 1.5 kV, whereas
the original sensitivity was 8.1 μm/+ 1.5 kV. Actuator #11 was
used for both sensitivity measurements. The device was then
life tested for 100 hours using ± 1.5 kV at 60 Hz. No change in
surface figure was observed.

VIII SUMMARY

From the five candidate actuator types presented in
the preceding chapters, the coherent stack device is the
leading candidate for further device development. This
type of actuator has exceeded all program goals (e.g.,
8 μm deformation at 1.5 kV and $\lambda/5$ pp for 100 hours at
12 μm total tilt between actuators). The bimorph and tube
devices have also performed well. For example, both types
provided a dilatation of 6 μm at 1.5 kV and exhibited good
stability during life testing. However, the bimorph requires
a redesign effort to reduce the number of parts. The tubular
actuator should undergo further investigation since its
ultimate potential was not fully exploited during the program.

The brief amount of data acquired for the honeycomb and
multilayer devices suggest that they represent very attractive
candidates for future test and evaluation. Although the
material and technology is available to produce them, these
actuators are not, at the present time, expected to be ready
for device implementation.

IX   SUGGESTIONS FOR FUTURE WORK

The results of this program provide a significant
data base upon which a full size mirror (20 cm) may be
designed and fabricated. There are, however, a small
number of considerations which require further develop-
ment in a follow-on program. These areas, which were
not completely pursued due to the brevity of the present
program, are discussed briefly below.

1   Temperature Stabilization

One of these areas concerns temperature stabilization
(i.e., athermalization) such that the optical figure remain
constant even though the ambient temperature varies. It
was demonstrated that close matching of thermal expansion
coefficients and careful use of the correct epoxy made a
distinct improvement in figure stability. However additional
athermalization engineering may be necessary for a full size
deformable mirror.

2   Mechanical Resonances

For the devices fabricated during the program, the
lowest resonant frequencies were all greater than 2 kHz.
Mechanical resonances will require further study to deter-
mine the frequency shift, if any, when proceeding to a
larger scale device. A full size mirror may employ dummy
actuators at the edge. The role played by this edge mount-
ing should also be investigated. The complex of face plate,
column and base plate resonances require analysis to deter-
mine the proper type of damping. A resonantly damped mirror
would become a truly broad band device wherein one deformable
mirror could be utilized as both a wave front corrector and
as a dither mirror.

3   Heat Exchange Faceplate

Further work should also include the effect that a

cooled face plate has upon the deformable mirror performance in terms of influence function, meshing, sensitivity, etc. The face plate should be examined from both a single pass and double pass approach. If the single pass solution provides insufficient cooling the double pass system may be a viable alternative by increasing the actuator force (e.g., by adding more layers). The variation of inlet and outlet pressure, as well as mechanical vibrations caused by the flow of coolant fluid, are additional areas which may necessitate an engineering effort.

4   Reliability

The ultimate reliability limits were not fully established during this program, although the attempt was made to exercise the deformable mirrors far in excess of their nominal operating points (e.g., 12 μm tilt between adjacent actuators for 100 hours rather than the program goal of 6 μm). Determining failure mechanisms, of course, requires failures in order to obtain statistical data. There were no such failures during the program. Future work should, therefore, require even greater excursions beyond the "standard" operating level in terms of applied voltage, driver frequency and duration of life test to ascertain device fatigue and failure points. Other bonding techniques, such as vacuum welding, should be investigated to achieve greater bonding strength in the coherent stack, even though a deliberate attempt to mechanically stress sample stacks resulted in ceramic breakage rather than epoxy failure.

5   Coatings

A final mirror design should embody the latest, state-of-the-art design to achieve the maximum device performance.

APPENDIX A

Resonance Measurement

Deformable surface devices are frequently examined
for resonances, which are measured by both optical and
electrical techniques. The optical procedure employs a
Fizeau interferometer such that the laser beam is modulated
at a frequency of 1 Hz less than the frequency of the driven
actuator. During the off-resonance mode only the fringes
in the vicinity of the driven actuator pulsate at a frequency
of 1 Hz. During resonance the entire fringe pattern vibrates
according to the particular allowed eigen mode. The results
of this experiment are visually noted and checked against the
electrical resonance measurements.

The electrical technique is diagramed in Figure A-1.
In this case an actuator is driven over a selected frequency
range, while another actuator is used to detect any change
in base line voltage at resonance. The sensor signal is
rectified and directed to the y-axis of a 2 dimensional
plotter, whose x-axis corresponds to the frequency of the
driven actuator. Our experience has shown that these
electrical and optical means of resonance detection yield
identical results and are complementary in that the optical
method permits mode type identification. Assuming a particular
sensor-actuator does not lie at a node, the signal derived
from this actuator locates the frequency of a resonance, but
does not yield type or intensity information since the derived
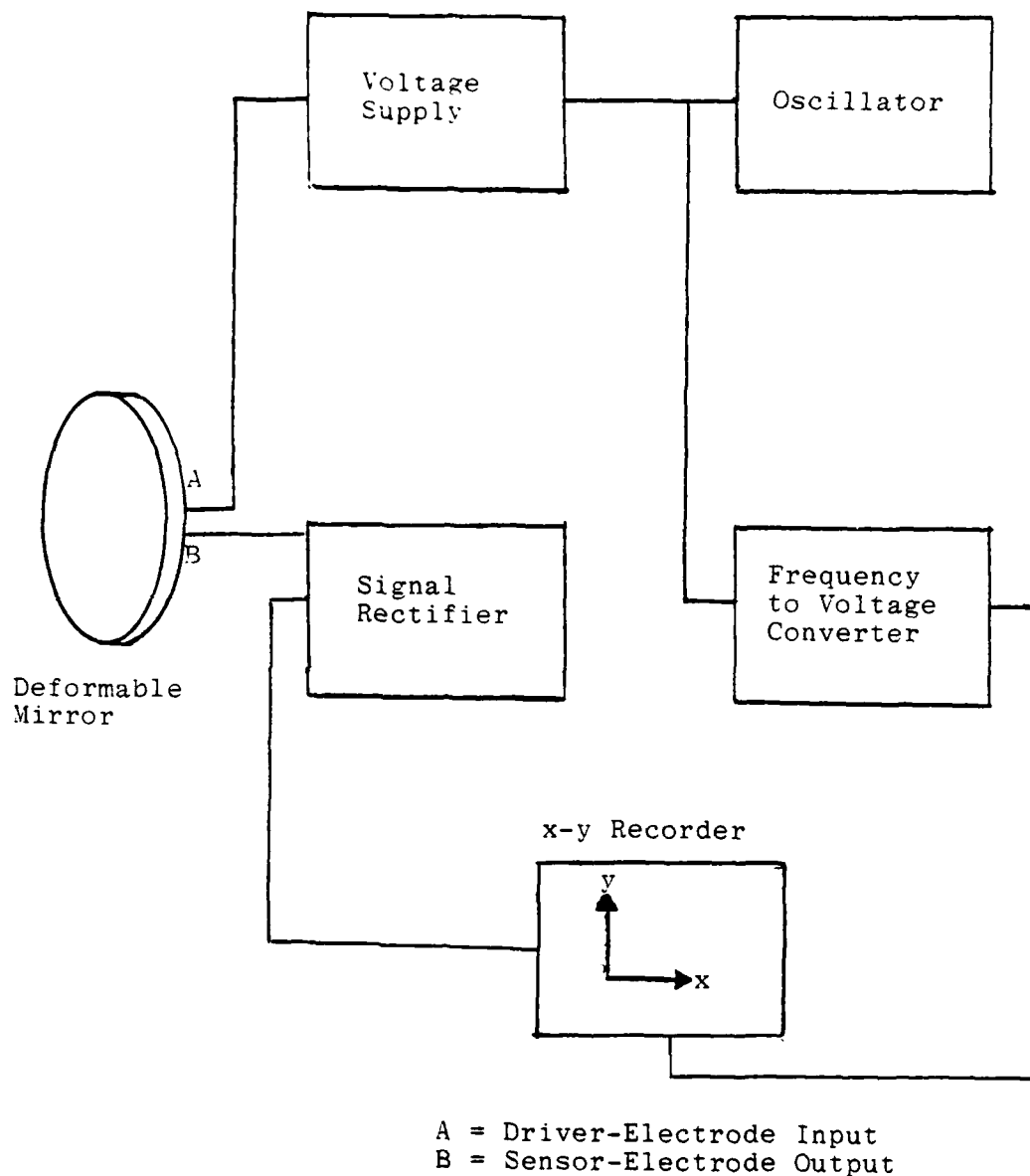voltage amplitude is dependent on the distance to a node.

A = Driver-Electrode Input
B = Sensor-Electrode Output

Figure A.1 - Resonance measuring using electrical sensing

62

APPENDIX B

MISCELLANEOUS

Occurring during the program were several ancillary
difficulties whose presentation in the principle technical
sections would have detracted from the primary emphasis.
These topics (discussed below) include vacuum welding
(section B.1), coherent stack delamination (B.2), moly-
bdenum face plates (B.3), creep test associated with mechanical
loading of an actuator (B.4) and low temperature solders (B.5).

B.1 Vacuum Welding

During this period we received vacuum welded samples of
PZT from our facilities at Applied Technology Division (ATD).
For comparison we also bonded together some PZT disks using
epoxy. Both ends of the bonded PZT disks were attached to
short rods to facilitate bond-breaking. We measured a tension-
shear type stress breakage point. It is felt that this particular
stress mode most closely resembles the situation encountered
when bending glass on a mirror. Table B-1 lists the results.

Samples 2 - 4 failed due to fracture in the PZT. Apparently
the indium bond is comparable with the epoxied samples. The
aluminum bond yielded distinctly inferior results. In the case
of samples #3 and #4 the presence of the frit may have played
a beneficial role. In general, these results show that vacuum
welding may provide a suitable alternative to epoxy bond in the
event that the "footprinting" problem is not sufficiently resolved
by control of faceplate bond thickness.

B.2 Coherent Stack Delamination

The fabrication of a 21 element, coherent stack device
led to an unanticipated problem. After bonding 20 disks of
PZT and bonding a plate of stainless steel (0.25 cm thick)
to each end of the stack, several delaminations occurred,

63

TABLE B-1.   RESULTS OF VACUUM WELDING

Vacuum Welded Samples

1. PZT-Aluminum-PZT
    (no silver-glass frit on PZT) - 26 Newtons

2. PZT-Indium-PZT
    (no silver-glass frit on PZT) - 249 Newtons

Epoxied Samples

3. PZT-Epoxy (cooper doped)-PZT
    (silver-glass frit on PZT) - 222 Newtons

4. Same as number 3 but no frit - 195 Newtons

each one at or in the vicinity of the fifth layer. In the
past we had bonded only 15 disks and had used no stainless
steel. However, nine stacks did survive and are now being
fabricated into a coherent stack device. We believe that
sufficient acoustic energy was generated by the saw cutting
through the stainless steel and that the length of the stack
permitted a condition of resonance (i.e., delamination at the
same point). We sliced a new coherent stack, which is
identical to the previous stack, except for the absence of the
stainless steel end plates. No delamination of the stacks
occurred.

B.3 Molybdenum Faceplates

One additional area of concern is the use of molybdenum
faceplates. During the program we have experienced waffling
and dish-bending of moly plates after repeated attempts at
moderate surface grinding. The plates on hand bow-in
somewhat uniformly as soon as the surface skin is broken, but
thereafter retain their shape during grinding. Annealing the
plates was unsuccessful in terms of removing internal stresses.
This problem can be solved by the purchase of thick plates
(2 - 3 times the mirror thickness) and simply grinding them
to the required thickness on the Lapmaster. This procedure
is somewhat tedious since removal rates average 25 µm per hour,
but is a sure process.

To obviate the necessity of time consuming surface grind-
ing during the program, glass faceplates were employed when
necessary. The thickness of the glass faceplate may be
scaled to determine the equivalent thickness of a molybdenum
faceplate. The relationship between a "nearly" point load (P),
applied to a face plate of thickness (T) and diameter (2a), and
the resulting deflection (W) is given by the following expression

65

found in Timoshenko's Treatise, "The Theory of Plates and Shells".

$$W = \frac{3(1-V)(3+V)Pa^2}{4\pi eT^3}$$

V = Poisson's ratio

e = Youngs modulus

Figure B-1 is a plot of applied load versus glass thickness for molybdenum and for glass face plates. A deflection of 6 μm is assumed. The ratio of glass thickness to molybdenum thickness for a given applied force is approximately 9:5 over the entire range of thickness. Thus, the scale factor of 9:5 may be employed to determine the sensitivity of a molybdenum face plate when the sensitivity of a glass face plate is known. The same actuator spacing and applied voltage is assumed.

B.4   Creep Test

Coherent stack actuators were subjected to static compressive mass loads of 14.5 kg/cm^2 for periods up to 24 hours. Changes of length of 0.1 to 6.3 μm were measured using an electronic micrometer in a temperature controlled environment. No consistent trend could be extrapolated from the data. Part of the problem is that the measuring probe has an accuracy of .03 μm but only for short times (~15 minutes) and the long term drift accuracy of the instrument was highly variable. Secondly the actuators tested appeared to vary in a nonreproducible fashion. For example, one actuator appeared to compress 2 μm in the first 12 hours, then show no further movement, while another appeared to compress less than 0.2 μm during the first 12 hours but compressed 1 μm during the next 12 hours. Thus no credence can be placed on the quantitative data. The best that can be said is that qualitatively, at these loads, which are five to ten times larger than those experienced by an
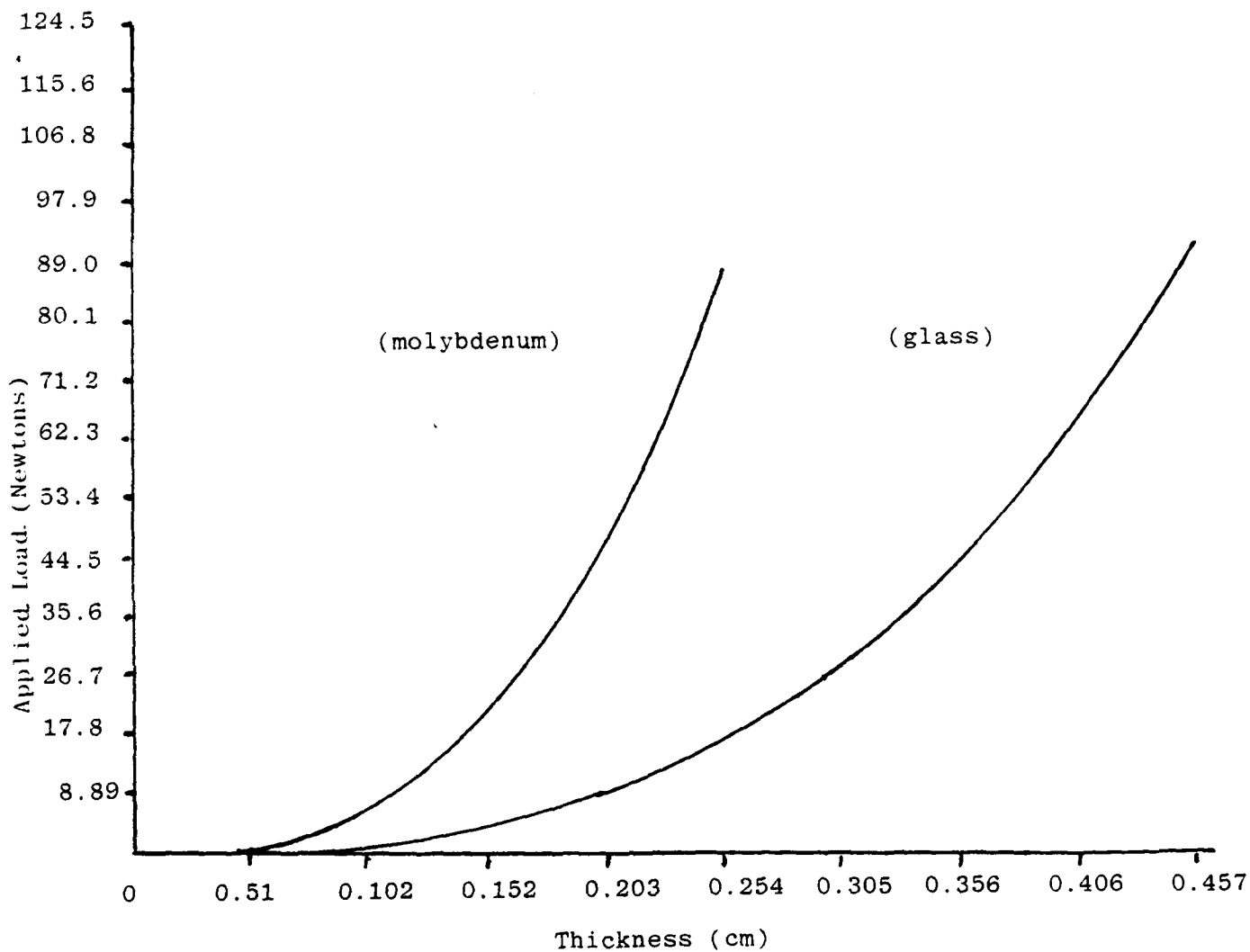
66

Figure B-1 - Applied load versus face plate thickness assuming a
deflection of 6 μm

67

actuator in a mirror of the type studied in this program, there appears to be some creep.

B.5 Low Temperature Solders

In order to circumvent the possiblity of creep in epoxies, we have investigated the use of low temperature solders. Chrome-gold was evaporated on the piezoelectric ceramic or on the silver frit. These surfaces could be bonded with an indium solder under a vacuum. The chrome-gold layer appears to have adhered well. However, the solder itself failed during stress measurements. Indicated bond strength is approximately 1/4 that of the best epoxies.

B.6 Influence Function Parameters

Deformable mirrors cast in the form of a continuous surface usually have influence functions which are very nearly gaussian in shape. The actual height of the function and function width are empirically determined by the glass thickness, actuator spacing and pusher geometry for a given actuator class. We did not attempt to model these parameters during the program but rather relied upon data and associated analysis generated from over 150 devices of various types fabricated and tested at Itek.

APPENDIX C

Capacitance Measurement

The various actuator types discussed in this report were
measured for capacitance and loss tangent by means of an
impedance bridge (General Radio, type 1650-A). This impedance
bridge, operated at a frequency of 1 kHz, includes five
bridges for measurement of inductance (L), capacitance (C)
and resistance (R) with a one percent accuracy over all ranges.
Also measured by this instrument is the loss tangent (D),
which is defined as the ratio of the resistance (R) divided
by the impedance (X). The bridge measures the loss tangent
with an accuracy of $\pm$ 5%.

DISTRIBUTION

AUL/LDE
DTIC/DDA
AFWL/SUL
AFWL/HO
AFWL/AR
AFWL/ARLB
AFWL/ARA
AFWL/ARAA
AFWL/ARAO
Official Record Cy/ARAA
Adaptive Optics Assoc., Inc.,
  Cambridge, MA
Aeronutronic Div Ford Aerospace &
  Communication Corp/Newport Beach
AFIT/Lib/WPAFB
AFOSR Dir of Mathematical & Info
  Sciences/Bolling AFB
AVCO-Everett Rsch Lab/Everett, MA
Boeing/Albuquerque
McDonnell-Douglas Astronautic Co/
  Huntington Beach
NRL/WashDC
NSWC/Silver Spring, MD
Perkin-Elmer Corp Electro-Optical
  Div/Norwalk, CT
RADC/OCSE/Griffiss AFB
Rockwell Int'l Corp/Rocketdyne Div/
  Canoga Park
SD/YAD/Los Angeles
W. J. Schaefer Assoc./Wakefield, MA
Science Applications, Inc./Arlington
SRI/Menlo Park
TRW/Redondo Beach
United Technologies Rsch Cntr/
  East Hartford
United Technologies Rsch Cntr/Optics
  & Applied Tech Labs/West Palm Beach
BDM Corp/Albuquerque
Charles Stark Draper Lab, Inc./
  Cambridge, MA
DARPA/Arlington
Gen Dynamics/Convair Div/San Diego
Gen Rsch Corp/McLean, VA
Hughes Acft Co./Culver City
Hughes Rsch Lab/Malibu
Itek Corp/Optical Sys Div/Lexington, MA
Lincoln Lab/MIT/Lexington, MA

Lockheed Msl & Space Co., Inc./
  Palo Alto
Lockheed Msl & Space Co., Inc./
  Sunnyvale
UofAZ Optical Sciences Cntr/Tucson
Univ of Dayton Rsch Inst/Dayton
US Army Msl R&D Cmd/Redstone Arsenal

LMED

-8